J. Fluid Mech. (1990), *vol.* 216, *pp.* 459–504
Printed in Great Britain

Large-amplitude wavetrains and solitary waves in vortices

By S. LEIBOVICH AND A. KRIBUS

Sibley School of Mechanical & Aerospace Engineering, Upson Hall, Cornell University, Ithaca, NY 14853-7501, USA

(Received 19 May 1989 and in revised form 16 January 1990)

Large-amplitude axisymmetric waves on columnar vortices, thought to be related to flow structures observed in vortex breakdown, are found as static bifurcations of the Bragg–Hawthorne equation. Solutions of this equation satisfy the steady, axisymmetric, Euler equations. Non-trivial solution branches bifurcate as the swirl ratio (the ratio of azimuthal to axial velocity) changes, and are followed into strongly nonlinear regimes using a numerical continuation method. Four types of solutions are found: multiple columnar solutions, corresponding to Benjamin's 'conjugate flows', with subcritical–supercritical pairing of wave characteristics; solitary waves, extending previously known weakly nonlinear solutions to amplitudes large enough to produce flow reversals similar to the breakdown transition; periodic wavetrains; and solitary waves superimposed on the conjugate flow that emerge from the periodic wavetrain as the wavelength or amplitude becomes sufficiently large. Weakly nonlinear soliton solutions are found to be accurate even when the perturbations they cause are fairly strong.

1. Introduction

This paper is concerned with axially symmetric standing wavetrains and solitary waves, without restrictions to infinitesimal or weakly nonlinear amplitudes, in inviscid incompressible vortex flows. Although the paper may be regarded strictly as a contribution to understanding of waves which may propagate on vortex cores, our motivation is the exploration of a conceptual picture of vortex breakdown given by Leibovich (1983) (and in a more widely accessible review in 1984, we shall designate either of these references as L).

In aerodynamic contexts, the global flow field causes impressed forcing on concentrated vortices embedded in it. Generally, the spatial scales of the forcing are large compared to scales associated with the vortex core. A conceptual model of vortex breakdown is promulgated in L, guided in part by laboratory experiments and in part by the weakly nonlinear 'trapped wave' theory of Randall & Leibovich (1973, referred to hereinafter as RL). In the scenario outlined in L, vortex breakdown is a process that involves a critical admixture of a strongly nonlinear axisymmetric wave propagating in a vortex 'waveguide ' having axially varying characteristics (and hence an axial pressure gradient), and a smaller asymmetric perturbation arising from instability of the big wave. The pressure gradient impressed by the waveguide does work on the axially symmetric wave, causing it to grow to large amplitude. The weakly nonlinear trapped-wave theory of RL indicates that wave growth of this sort leads to a positional instability of the wave: as it grows, it

propagates faster, and an equilibrium position cannot be established (with respect to a reference frame fixed by the waveguide) unless there is a mechanism for extraction of energy from the axisymmetric wave. RL invoked viscosity as a mechanism to dissipate wave energy. On the other hand, laboratory experiments (such as those done by Sarpkaya 1971 and by Faler & Leibovich 1977, 1978) show clear evidence of non-axisymmetric features within a nearly axisymmetric 'bubble' form of vortex breakdown, and the onset of asymmetry is consistent with an instability of the axially symmetric flow. If the 'bubble' were regarded as a manifestation of a large-amplitude, nearly axisymmetric wave, then instability to asymmetric perturbations offer the possibility of much larger energy transfers from the wave than would viscous dissipation. Furthermore, the features of vortex breakdown appear to depend little on viscosity, at least at higher values of the Reynolds number. Consequently, it is suggested in L that the required energy extraction from the strongly nonlinear axially symmetric wave arises by the transfer of its energy to azimuthally asymmetric modes of motion which arise by instability. (It is pointed out in L that a large-amplitude axially symmetric mode – large-amplitude implying a variation occurring on axial scales comparable with the vortex core radius – is required in vortex breakdown, since only this component of a Fourier decomposition in the azimuth can lead to the deceleration of fluid on the vortex axis that is the hallmark of vortex breakdown.) On the basis of their experimental observations in flows very different from those already cited, Maxworthy, Mory & Hopfinger (1983) also suggest, in a paper published in the same 1983 volume as the paper by Leibovich, that breakdown is associated with loss of stability of large axially symmetric waves to non-axisymmetric perturbations.

To explore this suggested process, we have divided it into elements which at a later time must be recombined. The first element is the large-amplitude axially symmetric wave, and the aim of this paper is to develop a better understanding of these waves. The other ingredients of the hypothesis, not yet considered, are loss of stability to asymmetric perturbations, and effects engendered by axial inhomogeneity caused by the global flow field. We emphasize that the phenomenon of vortex breakdown is unlikely to be attributed to only one physical mechanism, such as big axisymmetric waves: interacting mechanisms are almost certainly involved, and a satisfactory understanding of the phenomenon will depend on a proper synthesis of multiple interacting causes. In our view, already indicated, a promising minimal set of effects is indicated by experiment to be (i) large-amplitude waves, (ii) energy transfer from the big waves to equilibrated three-dimensional instabilities of modest amplitude, and (iii) axial variation caused by pressure gradients impressed on the vortex core. In completely confined flows, such as the class studied by Vogel (1968), Ronnenberg (1977), Escudier (1984), and Lugt & Abboud (1987), among others, viscous dissipation may be large enough (as originally assumed in RL) so that vortex breakdown may take place without three-dimensional instability (ingredient (ii)), and viscous diffusion may significantly augment pressure gradients (ingredient (iii)) which are caused by the deceleration required by the endwall.

In axially symmetric steady flow it is well known that the Euler equations for inviscid swirling flow may be reduced to a single elliptic differential equation for the stream function. This equation seems to have been first discovered by Bragg & Hawthorne (1950), and in this paper we shall refer to it by their names. Following Leibovich (1985), we parameterize the Bragg–Hawthorne equation (BHE) by the relative level of the swirl, and construct standing waves, either infinite wavetrains or

solitary waves, by studying the branching behaviours which arise as the parameter is varied (other, non-wavy flows, were discussed by Leibovich 1985 from this starting point, and a few of the results to be detailed here for weakly nonlinear wavy flows were announced in Leibovich 1987). The procedure can therefore be described as a search for static bifurcations of the BHE. Another natural parameterization that might have been chosen as a starting point for a bifurcation analysis is the wave speed of waves of permanent form. Here one adds a constant parameter to the primary axial velocity profile, given in a specific frame of reference, and regards the swirl as fixed. This choice, although more useful for some purposes than the parameterization using swirl level, introduces the wave-speed parameter into the problem in an awkwardly nonlinear way, and we have not made use of it in this work.

Branching, when it occurs, is from a primary columnar vortex, assumed to be given. The flows which bifurcate from this vortex are required to have the same volume flow rate, and the same total head and circulation variation with stream function as does the given vortex. With these constraints and the assumption that the flow is either periodic in the axial direction with a finite wavelength L or is columnar at upstream and downstream infinity, we find that new flow branches may be of four kinds. One class (I, discussed in §4) of bifurcating flows is again columnar, so there are no axial variations; a second class (II, §6) consists of solitary waves with the primary flow at upstream infinity; periodic wavetrains comprise the third class (III, §5); and a fourth class (IV, §5) consists of solitary waves that approach a columnar flow at large axial distances that is distinct from the primary columnar flow.

The columnar branches, of which there is an infinite number, when taken together with the primary flow, are the 'conjugate' flows defined and discussed in Benjamin's (1962) seminal paper. Two of these are especially important and receive emphasis in Benjamin's work; these are the primary flow, and what we shall call the principal conjugate flow, which is the columnar flow branching at the principal, or lowest, eigenvalue of the linearized problem, and therefore differing from the primary flow by an azimuthal vorticity that does not change sign. The procedure adopted here allows one to determine how these solutions are interrelated. We are also able to show that, at a columnar–columnar bifurcation point between the primary flow and its principal conjugate, there is a transfer of Benjamin's (1962) criticality classification of the flows. That is, if one flow is supercritical on one side of the bifurcation point (does not admit upstream-propagating waves of infinitesimal amplitude, and shorter standing waves), then the other columnar branch is subcritical (admits upstream-propagating waves), and that these properties of the branches are exchanged as the bifurcation point is passed. (NB. We use some of the language of bifurcation theory, but our use of the terms 'supercritical' and 'subcritical' is according to Benjamin's wave classification, and is not related to the direction of bifurcation.)

Fully nonlinear solutions have been determined numerically. This of course requires that specific examples of primary vortices be considered. We have chosen one family of examples, uniform axial velocity and the Burgers vortex. While the uniform axial velocity of this primary vortex differs from the jet-like character of flows in which vortex breakdowns have been observed, the principal columnar flows which bifurcate from our example are either jet-like or wake-like depending on swirl level, and therefore closely resemble flows upstream or downstream, respectively, of vortex breakdown. (These flows correspond to different problems, having different angular and axial momenta and therefore cannot be imagined to be end states

somehow linked together in a single flow in a constant-area tube.) In addition to the general results on columnar branches already mentioned, we note here an interesting – though academic – feature of the principal columnar branch. We have found that this branch can be numerically continued to very small swirl levels. With this clue as a point of departure, we find the flow (in Appendix B) in the limit of vanishing swirl by asymptotic means, showing that continuation to zero swirl is possible.

Numerical examples of fully nonlinear wavy solutions similar to some of those discussed in this paper have been presented by Hafez *et al.* (1987) (an abbreviated account is given by Hafez & Salas 1985). Our paper gives a considerably more comprehensive picture of the inviscid picture by identifying classes of solutions other than periodic wavetrains, and by uncovering the connections between them. The results of Hafez *et al.* were computed for a different (although more or less similar) class of primary vortices, yet their results are qualitatively similar to ours. This, and the theoretical argument of this paper, leads us to believe that the response to variation of swirl, and the main characteristics of the flows to be described here, are not the consequence of a special choice of profiles for the numerical work, but are of general applicability.

Solitary waves of class II can be found for the supercritical values of parameters by numerically continuing known weakly nonlinear solitary waves (with our choice of primary vortex, we have access to weakly nonlinear results found by Leibovich 1970 which we use as a starting point) to large amplitude. These solitary-wave flow fields approach the primary columnar flow asymptotically at large upstream and downstream distances. Their amplitudes can be increased to values sufficiently large to cause stagnation points to appear, followed by encapsulated regions of closed streamlines. The utility of the results when flow reversals are present requires careful consideration, particularly since added non-uniqueness enters in such circumstances, and the consistency requirement of the Prandtl–Batchelor criterion is violated. We believe that the results will prove to be of value at these large amplitudes, and discuss the reasons for this belief in §5.2. An interesting and potentially useful point is that even at amplitudes large enough to cause stagnation and reversed flow, the weakly nonlinear solitary-wave solutions remain a good approximation to the results of the fully nonlinear calculations.

For subcritical parameter values, periodic wavetrains (class III) have been found by numerical continuation beginning with infinitesimal waves. As the amplitudes of the periodic wavetrains increase at fixed wavelength in the numerical examples (as they do when the parameter measuring swirl increases), the wave troughs become highly localized, and the wave crests become very broad. These broad crests have virtually no axial variation, that is, they are nearly columnar. We show that these nearly columnar flows closely approximate, at large wave amplitude, the columnar principal conjugate vortex. The same kind of behaviour is found to hold when the swirl level is held fixed, but the wavelength of a wavetrain is increased. In either case, an individual wave trough approaches a solitary wave with the principal conjugate columnar vortex being the flow at 'large' distances upstream and downstream. Thus, we are led to another family of solitary waves (class IV) distinct from those supported by the primary vortex, but clearly related to it through branching.

2. Problem formulation

The Euler equations in cylindrical coordinates (r, θ, z) for steady, incompressible, axially symmetric flow may be reduced to a single elliptic partial differential equation for the Stokes stream function, ψ, related to the radial (u) and axial (w) velocity components by

$$u = -r^{-1}\psi_z, \quad w = r^{-1}\psi_r.$$

The equation, which connects the azimuthal vorticity to the total head and circulation, seems to have been first found by Bragg & Hawthorne (1950) and is given by

$$\mathrm{D}^2\psi = r^2 H'(\psi) - FF'(\psi), \tag{BHE}$$

where

$$\mathrm{D}^2\psi \equiv \psi_{rr} - r^{-1}\psi_r + \psi_{zz} = r\eta$$

and η is the azimuthal component of vorticity. A number of other authors have made use of this equation, notably Long (1953), Fraenkel (1956), Squire (1956), and Benjamin (1962). More recent examples of the use of this equation, with specific application to the problem of vortex breakdown, have been given by Keller, Egli & Exley (1985) and by Fiedler & Rotunno (1986). See Batchelor (1967) for a convenient reference for a derivation of BHE, following Bragg & Hawthorne, or Yih (1965) for a derivation by an alternative method. The replacement of the Euler equations by BHE is justifiable at all points in a steady, inviscid and axially symmetric flow with the possible exception of meridional stagnation points (i.e. where $u = w = 0$, but v, the azimuthal velocity component, may be non-zero), which are singular points of the transformation. In BHE, $H(\psi)$, the total head or Bernoulli function

$$H(\psi) = \frac{1}{\rho}p + \tfrac{1}{2}\boldsymbol{v}\cdot\boldsymbol{v}, \tag{1}$$

and $F(\psi)$, the circulation about the symmetry axis (apart from a factor of 2π),

$$F(\psi) = rv(r, z) \tag{2}$$

are functions of ψ alone. That F is a function of ψ alone is a consequence of conservation of angular momentum in an inviscid fluid.

Solutions to BHE are solutions to the Euler equations under the stated restrictions, and different inviscid flow problems arise from the specifications of the pair of functions H and F. The simplest cases are those for which the radial component of velocity vanishes at some plane $z = z_1$ on which the axial (w) and azimuthal (v) velocity components are specified to be $W(r)$, $V(r)$ with $W \neq 0$; then $H'(\psi)$ and F are easily determined (see Benjamin 1962). In this case, which we consider here,

$$\frac{1}{\rho}\frac{\partial p}{\partial r} = \frac{V^2(r)}{r} \tag{3}$$

at this plane. Since

$$\psi(r, z_1) = \int_0^r rW(r)\,\mathrm{d}r \equiv \Psi(r) \tag{4}$$

we can suppose this latter relation to be inverted to give

$$r = R(\psi). \tag{5}$$

This inversion can always be done (in principle) if $W(r) \neq 0$. At $z = z_1$, we can now regard W as a function of ψ, since

$$W = \frac{1}{r}\frac{\mathrm{d}\psi}{\mathrm{d}r}(r, z_1) = \frac{1}{R(\psi)}\frac{\mathrm{d}\Psi}{\mathrm{d}R}(R(\psi)). \tag{6}$$

With $V(r)$ prescribed, $F(\psi)$ is determined to be

$$rV \equiv F(\psi) = R(\psi)\, V(R(\psi)). \tag{7}$$

The pressure may now be found as a function of ψ from (3) by integration,

$$\frac{1}{\rho}p = \frac{1}{\rho}p(0, z_1) + \int_0^{R(\psi)} \frac{V^2(r)}{r}\mathrm{d}r, \tag{8}$$

and thus $H(\psi)$ may be identified. If the radial velocity is not given to be zero at $z = z_1$, but is prescribed as some non-trivial function of r, a similar construction of $H(\psi)$, $F(\psi)$ can be carried out. We call the flow given at the plane $z = z_1$ the 'specifying flow'; this will be taken to be the basic, or primary, flow and the starting point of our investigations.

Only $H'(\psi)$ is required for the analysis, $H(\psi)$ itself is not needed. At a plane $z = z_1$ where $u = 0$, $v = V$, $w = W$,

$$\frac{\mathrm{d}H}{\mathrm{d}\psi} = \frac{\partial H}{\partial r}\frac{\mathrm{d}R}{\mathrm{d}\psi} = \frac{1}{R^2}F\frac{\mathrm{d}F}{\mathrm{d}\psi} + \frac{1}{R}\frac{\mathrm{d}W}{\mathrm{d}R}. \tag{9}$$

Now we suppose that, at $z = z_1$, the functional form of the swirl $V(r)$ is fixed, but the level is adjustable, so that

$$F(\psi) = \lambda f(\psi), \tag{10}$$

where f is a fixed function, and λ is an adjustable constant. BHE for ψ may be written

$$\mathrm{D}^2\psi = r^2 A(\psi) - \lambda^2 B(\psi, r^2) \tag{11}$$

where $$A(\psi) = \frac{1}{R(\psi)}\frac{\mathrm{d}W}{\mathrm{d}r}(R(\psi)), \quad B(\psi, r^2) = (R^2(\psi) - r^2)ff'(\psi)/R^2(\psi). \tag{12}$$

With the appropriate interpretation of λ, we may regard (11) as dimensionless. Thus, if we scale distances by a characteristic radius b (such as that of a bounding tube, or, alternatively, the location of the maximum swirl speed), the specifying axial velocity by a characteristic speed W_0 (such as its value on the axis), the stream function by $b^2 W_0$, the azimuthal speed by a typical value V_0 (such as the maximum occurring in the flow), then

$$\lambda = \frac{V_0}{W_0}.$$

and we may interpret (11) as a dimensionless equation.

The parameter λ appears only as λ^2, and so we replace it hereafter with

$$\Lambda = \lambda^2, \tag{13}$$

and as a consequence of its definition, only admit positive values of Λ.

Suppose the boundaries of the fluid in the (r, z)-plane have, as two constituents, the

impermeable cylinders $r = r_i$ and $r = 1 > r_i$ (here we have chosen the outer tube radius as lengthscale for our problem). The columnar specifying flow

$$\psi(r, z) \equiv \Psi(r) \tag{14}$$

is a solution of (11) holding for all $\Lambda > 0$. We now wish to find other solutions, periodic in z with a prescribed wavelength L. Since both the specifying columnar flow and any other wave-like solutions that may exist simultaneously satisfy the same mathematical problem, and one possibility for this to occur is by bifurcation of new branches of solutions from the specifying flow, the multiple solutions so obtained, when of small amplitude, may be identified as the waves propagating on the specifying flow previously found in the literature (cf. Long 1953; Fraenkel 1956; Squire 1956; Benjamin 1962). Let

$$\Phi = \psi - \Psi(r), \tag{15}$$

represent the perturbation stream function. If there are other solutions, there is a z-periodic non-trivial solution to the (elliptic) partial differential equation

$$\mathrm{N}(\Phi, \Lambda) = \mathrm{D}^2\Phi + \Omega(\Phi, r, \Lambda) = 0, \tag{16a}$$

where

$$\Omega(\Phi, r, \lambda) = \Lambda P(\Phi, r) - r^2 Q(\Phi) \tag{16b}$$

with $$P(\Phi, r) \equiv B(\Psi + \Phi, r^2) - B(\Psi, r^2), \quad Q(\Phi) \equiv A(\Psi + \Phi) - A(\Psi),$$

satisfying the boundary conditions

$$\Phi(r_i, z) = \Phi(1, z) = 0, \tag{16c}$$

$$\Phi(r, z - \tfrac{1}{2}L) = \Phi(r, z + \tfrac{1}{2}L). \tag{16d}$$

The nonlinear problem admits solutions even in z, and we focus on these. In addition to admitting solutions with this symmetry ($z \to -z$), solutions are also admitted with $z \to z + h$, for any h. Thus, smooth z-periodic solutions may be constructed by appropriately piecing together (by reflections and shifts) solutions satisfying the Neumann boundary conditions,

$$\frac{\partial \Phi}{\partial z}(r, 0) = \frac{\partial \Phi}{\partial z}(r, \tfrac{1}{2}L) = 0. \tag{16e}$$

3. Static bifurcation analysis

The Bragg–Hawthorne equation describes only steady, or 'static', solutions. It can therefore be used to describe branches of the families of steady solutions corresponding to the same functional forms (as functions of the stream function) for the total head and circulation, and the same volume rate of flow. The bifurcation and continuation of such branches is discussed in this section. The question of the stability of the various solution branches of the BHE is a dynamical problem. This cannot be answered in the context of the BHE equation, and it is necessary to return to the Euler equations in which solutions to BHE are embedded. This is addressed (for columnar solutions only) in §4.

3.1. *Perturbation expansion*

We know that the specifying flow, $\Phi \equiv 0$, is a solution to the problem (16) for any value of the parameter Λ. This can fail to be a unique solution branch for a given Λ

only when $L(0, \Lambda)$, the operator defined by the linearization of $N(\Phi, \Lambda)$ about $\Phi = 0$, is not invertible. This occurs only when the parameter Λ coincides with an eigenvalue μ (say) for the linearized problem

$$L(0, \Lambda)\,\phi_0 \equiv D^2\phi_0 + \frac{\partial \Omega}{\partial \Phi}(0, r, \Lambda)\,\phi_0$$

$$= D^2\phi_0 + \left[\Lambda \frac{\partial P}{\partial \Phi}(0, r) - r^2 \frac{dQ}{d\Phi}(0)\right]\phi_0 = 0, \tag{17a}$$

$$\phi_0(r_i, z) = \phi_0(1, z) = 0, \quad \phi_0(r_i, z - \tfrac{1}{2}L) = \phi_0(r_i, z + \tfrac{1}{2}L). \tag{17b}$$

For Λ near an eigenvalue μ, we construct a solution branching from the specifying flow in a perturbation series. This will provide a local approximation for the solution branching at μ, which we shall continue numerically to larger values of $|\Lambda - \mu|$. Let

$$\Phi = \epsilon(\phi_0 + \epsilon\phi_1 + \ldots), \tag{18a}$$

$$\Lambda(\epsilon) = \mu + \epsilon\kappa(\epsilon) = \mu + \epsilon(\kappa_0 + \epsilon\kappa_1 + \ldots), \tag{18b}$$

and set

$$p_k(r) = \frac{1}{k!}\frac{\partial^k P}{\partial \Phi^k}(0, r), \quad q_k(r) = \frac{1}{k!}\frac{d^k Q}{d\Phi^k}(0), \quad s_k(r; \mu) = \mu p_k(r) - r^2 q_k(r), \tag{19a, b, c}$$

where μ refers to any eigenvalue of the linearized problem (17) and ϕ_0 the corresponding eigenfunction, ϵ is a small ordering parameter measuring the amplitude of the bifurcating solutions and the difference between Λ and its value μ at the bifurcation point, and the dots stand for higher-order terms in ϵ. When these relationships are substituted into (16a), Taylor series expansions in powers of ϵ carried out and each coefficient in the series set to zero, the first three coefficients are

$$L(0, \mu)\,\phi_0 = D^2\phi_0 + [\mu p_1(r) - r^2 q_1(r)]\,\phi_0 = 0, \tag{20a}$$

$$L(0, \mu)\,\phi_1 = -\{\kappa_0 p_1(r)\,\phi_0 + s_2(r; \mu)\,\phi_0^2\}, \tag{20b}$$

$$L(0, \mu)\,\phi_2 = -\{\kappa_1 p_1(r)\,\phi_0 + \kappa_0 p_1(r)\,\phi_1 + \kappa_0 p_2(r)\,\phi_0^2 + 2s_2(r; \mu)\,\phi_0\phi_1 + s_3(r; \mu)\,\phi_0^3\}, \tag{20c}$$

and all the ϕ_n satisfy the same boundary conditions (17b).

Note that

$$p_1(r) \equiv \frac{1}{r^3 W^2(r)}\frac{df^2}{dr}, \quad q_1(r) \equiv \frac{1}{rW}\frac{d}{dr}\left(\frac{1}{r}\frac{dW}{dr}\right).$$

The numerator of $p_1(r)$, when multiplied by Λ, is Rayleigh's discriminant, and therefore sensible problems, in the context of considerations such as in this paper, will have $p_1(r) > 0$, and we assume this to be the case. (Otherwise, the primary flow is unstable.) Only positive values of μ can correspond to branch points, since $\Lambda > 0$ by definition. If $p_1(r) > 0$ and $q_1(r) \geqslant 0$, then the smallest (or 'principal') eigenvalue is guaranteed positive (Leibovich 1985), and is therefore a possible branch point. Positive values of $q_1(r)$ are not necessary for this to be so. In the development below, we explicitly assume that the smallest eigenvalue is positive. If this is not so, then the mathematical changes needed are obvious – one deals only with the positive

eigenvalues, of which there is an infinite number – but a number of the results and interpretations given here may require modification.

The problems we have posed here depend on two parameters, Λ and L, once the specifying flow is selected.

The principal eigenfunction has no zeros in the interior of D (Courant & Hilbert 1953) and, without loss of generality, we therefore may take it to be non-negative. Even eigenfunctions are all of the form

$$\phi_0 = \chi_{pm}(r)\cos(2m\pi z/L), \tag{21}$$

where the integer index p is the number of internal zeros of $\chi_{pm}(r)$, which satisfies the problem

$$\left(r\frac{\mathrm{d}}{\mathrm{d}r}\right)\left(\frac{1}{r}\frac{\mathrm{d}\chi_{pm}}{\mathrm{d}r}\right)+\left[\mu_{pm}\,p_1(r)-r^2q_1(r)-\left(\frac{2m\pi}{L}\right)^2\right]\chi_{pm}=0, \tag{22}$$

$$\chi_{pm}(r_i)=\chi_{pm}(1)=0.$$

Here we have labelled the eigenvalues according to the indices p and m corresponding to the associated eigenfunction. The principal eigenfunction corresponds to $m = 0$ and to the index p, which we can take to be $p = 0$, such that the function $\chi_{00}(r)$ has no zeros internal to D. The principal eigenfunction belongs to the eigenvalue μ_{00} and is a function of r alone. A solution that branches from the principal eigenvalue therefore corresponds to a new columnar flow (which we shall call the 'principal conjugate branch' since it is a conjugate flow defined by Benjamin 1962), and an infinite number of other columnar flows (also conjugates in the sense of Benjamin) branch from larger eigenvalues corresponding to $m = 0$ and the eigenfunctions $\chi_{p0}(r)$, for $p = 1, 2, 3, \ldots$. Solutions periodic in z (standing waves) branch from eigenvalues corresponding to eigenfunctions with $m \neq 0$. Modes for all values of m are characterized by the number of zeros of their eigenfunctions with $\chi_{pm}(r)$ having p internal zeros.

The eigenvalue problem (17) is in standard Sturm–Liouville form (Courant & Hilbert 1953), and some of its features (such as bounds on the smallest eigenvalue) are discussed by Leibovich (1985). There is one comment which is worth making at this point about this eigensystem, in addition to the observations we have already made. Eigenvalues corresponding to z-dependent eigenfunctions (constituting 'wavy' modes, with eigenvalues exceeding μ_{00}), decrease as L increases (Courant & Hilbert 1953), and as $L \to \infty$, μ_{00} is an accumulation point for the wavy eigenvalues $\mu_{0m}, m \neq 0$. For the same reason, waves corresponding to higher radial modes have accumulation points, with $\mu_{pm} \to \mu_{p0}$ as $L \to \infty$.

3.2. *Branching behaviour*

If ϕ_0 is an eigensolution, then the solution to the adjoint eigenvalue problem with an unweighted inner product is ϕ_0/r, or alternatively, the problem is self-adjoint under the inner product

$$(F, G) = \langle FG \rangle,$$

where

$$\langle \cdot \rangle = \int_D r^{-1}(\cdot)\,\mathrm{d}r\,\mathrm{d}z,$$

and D is the spatial domain in which our problem is set.

For problem (20*b*) to have a solution ϕ_1, the solvability condition

$$\kappa_0 = -\frac{\langle s_2(r;\mu)\,\phi_0^3\rangle}{\langle p_1(r)\,\phi_0^2\rangle} \tag{23}$$

must be satisfied. If $\mu = \mu_{00}$ is the smallest eigenvalue, then ϕ_0 is the primary eigenfunction, which may be taken to be positive. Unless $\mu_{00}\,p_2(r) - r^2 q_2(r)$ is distributed in a special way, then κ_0 is non-zero and the bifurcation at μ_{00} occurs with finite slope (i.e. it is transcritical or $\mathrm{d}\Lambda/\mathrm{d}\epsilon \neq 0$ at $\epsilon = 0$).

The eigenfunction corresponding to μ_{01}, the lowest eigenvalue for $m = 1$, is

$$\phi_0 = \chi_{01}(r)\cos(2\pi z/L). \tag{24}$$

According to (23), $\kappa_0 = 0$ for solutions branching from $\mu_{0m}\,(m > 0)$, since the defining integrals extend over m periods in z and the numerator therefore vanishes. For $m = 1$, the differential equation determining ϕ_1, from (20*b*), is now

$$\begin{aligned} L(0,\mu)\,\phi_1 &= -[\mu_{01}\,p_2(r) - r^2 q_2(r)]\,\phi_0^2 \\ &= -\tfrac{1}{2}[\mu_{01}\,p_2(r) - r^2 q_2(r)]\,[1+\cos(4\pi z/L)]\,\chi_{01}^2, \end{aligned} \tag{25}$$

with solutions in the form

$$\phi_1 = f_1(r) + f_2(r)\cos(4\pi z/L). \tag{26}$$

The direction of the bifurcation is fixed now by κ_1. Assuming $\kappa_1 \neq 0$, $\Lambda(\epsilon) - \mu_{01} = \kappa_1\epsilon^2 + \ldots$, and the bifurcation there is a pitchfork ($\mathrm{d}\Lambda/\mathrm{d}\epsilon = 0$ and $\mathrm{d}^2\Lambda/\mathrm{d}\epsilon^2 \neq 0$ at $\epsilon = 0$). The value of κ_1 is determined by the solvability of (20*c*), and the formula corresponding to (23) is

$$\kappa_1 = -\frac{\langle 2s_2(r;\mu)\,\phi_0^2\phi_1 + s_3(r;\mu)\,\phi_0^4\rangle}{\langle p_1(r)\,\phi_0^2\rangle}, \tag{27}$$

and this does not generally vanish.

The solutions bifurcating at μ_{01} are wavetrains with wavelength L in an axially infinite region. By developing the series solution in ϵ, a finite-amplitude periodic wavetrain may be constructed.

When $L \to \infty$, $\mu_{01} = \mu_{00} + O(L^{-2})$, and the solution of the inhomogeneous ordinary differential equation for $f_1(r)$ is of $O(L^2)$. As a consequence, the series (18*a*) becomes disordered when $\epsilon L^2 = O(1)$. The way to deal with this non-uniform behaviour for long-waves by the method of multiple scales (or equivalent methods) is well-known. In the context of the approach taken here, the expansion is centred about the columnar bifurcation point, μ_{00}. The procedure, sketched in Leibovich (1987), goes as follows. Letting Z be the slow scale, with $Z = z\epsilon^{\frac{1}{2}}$, $\Phi = A(Z)\,\phi_0(r)$ (at lowest order), then $\phi_0(r)$ is the principal eigenfunction corresponding to the eigenvalue μ_{00}, and A satisfies the equation

$$\frac{\mathrm{d}^2 A}{\mathrm{d}Z^2} + \alpha A^2 + \beta\kappa_0 A = 0, \tag{28a}$$

where κ_0 is defined by (18*b*), as before, but is no longer restricted by the solvability condition (23), and

$$\alpha = \frac{\langle s_2\phi_0^3\rangle}{\langle\phi_0^2\rangle}, \quad \beta = \frac{\langle p_1\phi_0^2\rangle}{\langle\phi_0^2\rangle}. \tag{28b}$$

The analysis, although by a different route, is essentially that of Benjamin (1967).

Equation (28*a*) has the solitary-wave solution

$$A = a\,\mathrm{sech}^2\left[(\tfrac{1}{6}a\alpha)^{\frac{1}{2}}Z\right] = a\,\mathrm{sech}^2\left[(\tfrac{1}{6}a\epsilon\alpha)^{\frac{1}{2}}z\right], \tag{29a}$$

provided $a\alpha > 0$ (and has no such solution otherwise). The constant a in (29*a*) is related to the parameters in (28*a*); with the level of the extreme value of A set to be a and placed at $z = 0$, as has been done in (29*a*), the amplitude a, or more precisely, ϵa, is linearly related to the swirl rate by

$$\Lambda = \mu_{00} - \frac{2\alpha}{3\beta}\epsilon a. \tag{29b}$$

In this discussion, it has been assumed that ϵ is positive, so that waves of elevation or depression depend on whether a is positive or negative: since we must have $a\alpha > 0$, the question devolves to the sign of α, which is a functional of the specifying flow. Furthermore, since $\beta > 0$, (29*b*) shows that solitary waves may exist only for $\Lambda < \mu_{00}$. In this parameter regime, no infinitesimal standing waves are possible (since they all branch from eigenvalues greater than μ_{00}), and by definition this is a supercritical regime. Thus (29*b*) makes clear that weakly nonlinear solitary waves form only on supercritical flows. Further discussion of the criticality classification is given in §4.1.

The weakly nonlinear solitary-wave solutions found by Leibovich (1970) from the time-dependent Korteweg–deVries equation are equivalent to those given above. This alternative form effectively derives from the alternative parameterization of the time-independent problem by wave speed (instead of swirl level) mentioned in the Introduction and is

$$\Phi = \epsilon a\phi_0(r)\,\mathrm{sech}^2\left[\frac{1}{2}\left(\frac{c_1 a}{3c_2}\right)^{\frac{1}{2}}(z - c_0 t + \tfrac{1}{3}\epsilon a c_1 t)\right], \tag{30}$$

where a is an arbitrary amplitude, ϕ_0 is the eigenfunction of the linearized problem equivalent to (27), the c_i are constants depending on the base flow and ϕ_0 and are equivalent to α and β in (28). For a given base flow, the value of ϵa determines the wave amplitude and therefore its velocity; or, alternatively, the change in the base flow axial component that would make the solution stationary. Changing λ (that is, the azimuthal component) instead will produce the same results provided the swirl ratio is the same; so selecting an eigenvalue and setting λ (or Λ) completely determines this approximate solution.

The numerical construction of solutions along a branch can be done by a simple continuation method, starting with solutions generated numerically by the perturbation procedure described above.

3.3. *Branch continuation*

To 'continue' (Kubicek & Marek 1983 gives a good summary of continuation and bifurcation methods) a solution (Φ_0, Λ_0) known at a given value of $\Lambda = \Lambda_0$, to a neighbouring value differing from Λ_0 incrementally, we could proceed by taking Φ_0 as an initial guess for $\Phi(\Lambda_0 + \Delta\Lambda)$ in a suitable iterative procedure, such as Newton's method,

$$\Phi_{n+1} = \Phi_n - \mathrm{L}^{-1}(\Phi_n, \Lambda)\,\mathrm{N}(\Phi_n, \Lambda) \tag{31}$$

using an appropriate discretization for L and N. This will give a solution if L is not singular, that is, if no bifurcation or turning point is encountered, and if $\Delta\Lambda$ is sufficiently small. To increase the size of $\Delta\Lambda$ while still providing a good guess for the

iteration, we can proceed in the following standard way by differentiating along solution arcs $(\boldsymbol{\Phi}(\Lambda), \Lambda)$: since

$$\left.\begin{aligned} \mathrm{N}(\boldsymbol{\Phi}(\Lambda), \Lambda) &= 0, \\ \frac{\mathrm{dN}}{\mathrm{d}\Lambda}(\boldsymbol{\Phi}, \Lambda) &= \frac{\partial \mathrm{N}}{\partial \boldsymbol{\Phi}}\bigg|_{\boldsymbol{\Phi};\Lambda} \frac{\partial \boldsymbol{\Phi}}{\partial \Lambda} + \frac{\partial \mathrm{N}}{\partial \Lambda}\bigg|_{\boldsymbol{\Phi};\Lambda} = 0. \end{aligned}\right\} \tag{32a}$$

Then, at any point $(\boldsymbol{\Phi}, \Lambda)$, the 'slope' of the solution curve

$$\dot{\boldsymbol{\Phi}} \equiv \frac{\partial \boldsymbol{\Phi}}{\partial \Lambda} = -\left(\frac{\partial \mathrm{N}}{\partial \boldsymbol{\Phi}}\bigg|_{\boldsymbol{\Phi};\Lambda}\right)^{-1} P(\boldsymbol{\Phi}, r) = -\mathrm{L}^{-1}(\boldsymbol{\Phi}, \Lambda) P(\boldsymbol{\Phi}, r) \tag{32b}$$

assuming the linearized operator $\mathrm{L}(\boldsymbol{\Phi}, \Lambda)$ is invertible with inverse $\mathrm{L}^{-1}(\boldsymbol{\Phi}, \Lambda)$. We can think of (31) as a differential equation for $\boldsymbol{\Phi}$ as a function of Λ. We use (31) and (32*b*), in a numerical algorithm described in Appendix A, in a predictor–corrector mode. We first integrate (32), using a Runge–Kutta method to arrive at an estimate for $\boldsymbol{\Phi}$ at $\Lambda_0 + \Delta\Lambda$ assuming a solution is known at Λ_0, and then refine this estimate using Newton iteration (31). We begin each solution branch by using a three-term perturbation expression, also described in the Appendix, which is the discrete version of the analysis given in §3.2. This procedure will fail if secondary bifurcation points or turning points are encountered as a given branch is traced, and then a more involved procedure, such as that devised by Keller (1977) (see also Kubicek & Marek 1983) will be required. We did not encounter such complications in the course of our investigations.

To do detailed calculations, we must select a particular specifying flow. We take $r_1 = 0$, and explore the possible branches of solutions stemming from the following simple columnar vortex which has been previously treated by Leibovich (1970):

$$W(r) = 1, \quad V(r) = \lambda\{1 - \exp(-\alpha r^2)\}/r. \tag{33}$$

This example is known as the Burgers–Rott vortex. It corresponds to the following specifications of the functions arising in §2:

$$\left.\begin{aligned} &\Psi(r) = \tfrac{1}{2}r^2, \quad R(\psi) = 2\psi^{\frac{1}{2}}, \quad f(\psi) = 1 - \exp(-2\alpha\psi), \\ &A(\psi) = 0; \quad B(\psi, r^2) = (\psi - \tfrac{1}{2}r^2)\, 2\alpha \exp(-2\alpha\psi)\left\{\frac{1 - \exp(-2\alpha\psi)}{\psi}\right\}, \\ &P(\boldsymbol{\Phi}, r) = B(\tfrac{1}{2}r^2 + \boldsymbol{\Phi}, r^2) - B(\tfrac{1}{2}r^2, r^2); \quad \mathrm{Q}(\boldsymbol{\Phi}) = 0. \end{aligned}\right\} \tag{34}$$

3.4. *Numerical implementation*

The problem stated in (16) is discretized using central differences on a rectangular mesh in the meridional plane (r, z). Let $\boldsymbol{\Phi}, \mathbf{D}, \boldsymbol{\Omega}$ be the finite-dimensional counterparts of $\boldsymbol{\Phi}, \mathrm{D}^2, \Omega$, as defined in Appendix A; (16) then corresponds to the matrix equation

$$\mathbf{D}\boldsymbol{\Phi} + \boldsymbol{\Omega}(\boldsymbol{\Phi}, \Lambda) = 0. \tag{35}$$

Equation (35) is the basis for the numerical treatment. We do not discretize steps of the analytical procedure separately; rather, we provide an equivalent analysis for the approximate equation (35). A separate discretization of (22), for example, leads to eigenvalues that are slightly different than the bifurcation points of (35), and this is enough to prevent convergence to a solution branch in some cases. Even more telling, if eigenvectors obtained from the algebraic eigenvalue problem are used in conjunction with a semianalytic enforcement of an orthogonality condition (for

example, by means of a numerical quadrature), then the result will not be precisely orthogonal in the algebraic problem, and if the next stage of the problem is solved algebraically, errors are introduced. We therefore rederive equations (17)–(29) in the Appendix A for the algebraic system (35). This ensures consistency of numerical values throughout the analysis.

The strategy is the same as that described in §§3.2 and 3.3. First, a solution point on a non-trivial branch is sought using a perturbation expansion (or, for the solitary-wave branch, the weakly nonlinear solution may be used). Numerical integration of the discrete analogue of (32*b*) continues the branch away from the bifurcation point, and Newton's iterations serve as corrector steps at selected points along the branch.

4. Columnar–columnar bifurcations and continuation

In this section, we discuss some general questions about bifurcations of the specifying columnar flow to other columnar flows, give numerical results for the example specified in (34), and briefly discuss some aspects of the stability of the computed flows.

4.1. *Transfer of criticality condition*

Benjamin (1962) has provided a simple test to determine whether a given columnar vortex is subcritical or supercritical. As Leibovich (1979) has shown, this turns out to be an appropriate test (for axisymmetric disturbances) even though the crucial quantity determining whether upstream propagation of disturbances is possible is the group, not the phase, speed. Subcritical flows can be expected to be influenced by small downstream disturbances. This might be true even in flows that are supercritical according to this classification scheme, since it does not cover non-axially symmetric perturbations, but the propagation characteristics of non-axially symmetric waves (see Leibovich, Brown & Patel 1986) are more difficult to determine. Benjamin's criticality classification is important because it seems to be useful in correlating vortex breakdown data (see L), as Squire (1960) and Benjamin (1962) had proposed. In particular, the evidence (see Leibovich 1978 or L) indicates that flows upstream of vortex breakdowns are supercritical, while the (mean) flows downstream are subcritical.

To determine the criticality condition of a given columnar flow, we ask whether it can sustain infinitesimal waves of the form

$$\phi = \chi(r)\,\mathrm{e}^{\mathrm{i}kz}, \tag{36}$$

which means that equation (16*a*) has a solution in the form

$$\Phi + \epsilon\phi$$

for infinitesimal ϵ. This leads to a problem similar to that in §3.1, except that we wish to consider columnar flows other than the specifying flow (which has $\Phi = 0$), and, rather than fixing the wavelength ($= L$) and searching for values of Λ for which the linearized problem is solvable, the question is turned around: Λ is fixed, and we ask if there is any real value of k ($= 2\pi/L$) for which the linearized problem is solvable. If so, a standing wave with wavenumber k determined is possible and the flow is subcritical. If not, the flow is supercritical. Let

$$\hat{\mathrm{L}}(\Phi, \Lambda)(\,) = \frac{\partial^2(\,)}{\partial r^2} - \frac{1}{r}\frac{\partial(\,)}{\partial r} + \left[\Lambda \frac{\partial P}{\partial \Phi}(\Phi, r) - r^2 \frac{\mathrm{d}Q}{\mathrm{d}\Phi}(\Phi)\right](\,), \tag{37}$$

then we may write the differential equation for the small wavy perturbations as

$$-\frac{\partial^2\phi}{\partial z^2} = k^2\phi = \hat{\mathrm{L}}(\Phi, \Lambda)\phi. \tag{38}$$

We now regard this as an eigenvalue problem for k^2, with Λ fixed. It is, owing to (36), an ordinary differential equation for χ in standard Sturm–Liouville form and subject to the boundary conditions $\chi(r_1) = \chi(1) = 0$.

We know that the specifying flow is supercritical for $\Lambda < \mu_{00}$ (because there are *no* eigenvalues of (17) in this range of Λ, either corresponding to columnar flows or to wavy flows, according to §3.1), and subcritical for $\Lambda > \mu_{00}$, because, according to the observation of §3.1, there is a wave with *some* wavenumber for each value of $\Lambda > \mu_{00}$, with waves with arbitrarily long wavelengths branching off as $\Lambda \to \mu_{00}$ from above. If $\Lambda = \mu_{00}$, it is clear that the eigenvalue k^2 of (38) vanishes, and we may summarize by observing that the eigenvalue k^2 of (38) is negative if $\Lambda < \mu_{00}$, zero for $\Lambda = \mu_{00}$, and positive for $\Lambda > \mu_{00}$, and that

$$\frac{\mathrm{d}k^2}{\mathrm{d}\Lambda} > 0 \quad \text{at} \quad \Lambda = \mu_{00}.$$

We wish to characterize the criticality condition of the columnar vortex branching off from the specifying flow at $\Lambda = \mu_{00}$, on either side of the bifurcation point. To explore this, we differentiate (38) with respect to Λ, to arrive at an inhomogeneous equation for $\partial\chi/\partial\Lambda$:

$$\hat{\mathrm{L}}(\Phi, \Lambda)\frac{\partial\chi}{\partial\Lambda} - k^2\frac{\partial\chi}{\partial\Lambda} = \frac{\mathrm{d}k^2}{\mathrm{d}\Lambda}\chi - \frac{\mathrm{d}\hat{\mathrm{L}}(\Phi, \Lambda)}{\mathrm{d}\Lambda}\chi, \tag{39a}$$

where

$$\frac{\mathrm{d}\hat{\mathrm{L}}(\Phi, \Lambda)}{\mathrm{d}\Lambda}\chi = \frac{\partial\Phi}{\partial\Lambda}\left[\Lambda\frac{\partial^2 P}{\partial\Phi^2}(\Phi, r) - r^2\frac{\mathrm{d}^2 Q}{\mathrm{d}\Phi^2}(\Phi)\right]\chi + \frac{\partial P}{\partial\Phi}(\Phi, r)\chi. \tag{39b}$$

Since χ satisfies (38), (39) is solvable only if

$$\frac{\mathrm{d}k^2}{\mathrm{d}\Lambda} = \frac{\left\langle \chi\dfrac{\mathrm{d}\hat{\mathrm{L}}(\Phi, \Lambda)}{\mathrm{d}\Lambda}\chi \right\rangle}{\langle\chi^2\rangle}. \tag{40}$$

We are interested in (40) at $\Lambda = \mu_{00}$, $\Phi = 0$. The numerator of (40) is

$$\langle\chi^2\{2s_2(r, \mu)\dot{\Phi} + p_1(r)\}\rangle, \tag{41}$$

which we have used the notation of (21) and (23*b*). The only difference in (40), when evaluated at the bifurcation point for either of the intersecting solution curves is the direction, $\dot{\Phi}$, of the particular solution curve along which $\mathrm{d}k^2/\mathrm{d}\Lambda$ is evaluated. On the specifying flow, $\partial\Phi/\partial\Lambda = 0$, and on the second branch $\dot{\Phi} = \chi$, the eigenfunction, apart from an arbitrary multiplicative constant which we take to be unity. Thus, along the specifying flow, (40) reduces to

$$\frac{\mathrm{d}k^2}{\mathrm{d}\Lambda} = \frac{\langle p_1(r)\chi^2\rangle}{\langle\chi^2\rangle}. \tag{42}$$

To calculate the numerator of (40) for the non-trivial bifurcating solution, we differentiate (32*a*) twice with respect to Λ. The result, when evaluated at $\Phi = 0$, $\Lambda = \mu_1$, is

$$\hat{\mathrm{L}}(0, \mu_{00})\,\ddot{\Phi} + 2\mu_{00}\, s_2(r, \mu_{00})\,\dot{\Phi}^2 + 2p_1(r)\,\dot{\Phi} = 0,$$

and solvability for $\ddot{\Phi}$ requires

$$\langle \dot{\Phi}^2 \{2s_2(r, \mu_{00})\,\dot{\Phi} + 2p_1(r)\} \rangle = 0. \tag{43}$$

Combining (43) with (41), we find that on the bifurcating branch

$$\frac{\mathrm{d}k^2}{\mathrm{d}\Lambda} = -\frac{\langle p_1(r)\,\dot{\Phi}^2 \rangle}{\langle \dot{\Phi}^2 \rangle} = -\frac{\langle p_1(r)\,\chi^2 \rangle}{\langle \chi^2 \rangle}, \tag{44}$$

which is just the negative of (42). Therefore, since k^2 increases through zero as Λ increases through μ_{00} on the specifying flow branch, it must decrease through zero as Λ increases through μ_{00} on the principal branching solution.

Thus, we have shown that the criticality conditions holding on the specifying flow and that holding on the flow branching transcritically from it are transferred at the bifurcation point: this will be illustrated in §4.2. If we hold Λ fixed, our problem conforms to that considered by Benjamin (1962), who labels each columnar flow distinct from the specifying flow – and there may be more than one depending on the value of Λ – as 'conjugate' to the specifying flow. Benjamin shows that, if the primary flow is supercritical, then *all* conjugate flows must be subcritical. This conclusion has been confirmed by Fraenkel (1967), and is consistent with the local results of this section.

Recently, it has been claimed by Keller *et al.* (1985) that the analyses referred to above are incomplete, and that supercritical flows need not have subcritical conjugates. We think that different conclusions are reached because different problems are being addressed, and different meanings are being assigned to the words 'conjugate' flows. By this term we mean multiple solutions of the BHE having a fixed specification of the functional forms of the circulation $\Gamma(\psi)$ and the total head derivative $H'(\psi)$. Thus, we are talking about multiple solutions of only one nonlinear elliptic partial differential equation. Furthermore, we are dealing with a single fluid occupying the same flow domain both upstream and downstream and satisfying the BHE everywhere. If Γ and H have continuous first and second derivatives, the results stated above are consequences of satisfying the BHE. We see two ways to understand how Keller *et al.* (1985) can arrive at a conflicting conclusion. In both, their allowance of a finite region of *stagnant* fluid is essential. A review of the derivation of the BHE, which involves integration along streamlines, shows that the BHE need not hold at stagnation points (as already mentioned in §2), nor in a stagnant region. With this interpretation, Keller *et al.* (1985) do not impose the BHE for the entire body of fluid. There then is no conflict in the two results, which correspond to two distinctly different problems. In the second interpretation, the downstream conjugate state in Keller *et al.* (1985) is required to satisfy a BHE equation, but in the interior of the stagnant region it is necessary to choose $H'(0) = 0$ to ensure the flow is stagnant within the free streamline. In the downstream flow exterior to the stagnation zone, $H'(\psi) \neq 0$ in the limit $\psi \to 0$. Consequently, the first derivative of $H(\psi)$ is discontinuous in the downstream flow field, but is continuous

upstream. In this case, the upstream flow satisfies one BHE, and the downstream satisfies another, subtly different, BHE, and again the conflict is resolved.

The aim of this paper is to clarify the nature of the multiple solutions of the BHE, and the relationships between these solutions, with particular emphasis on standing wave solutions. In this regard, the principal conjugate, although not a 'wave-like' solution itself, will be shown in the next section to play a special role for solitary waves (our class IV flows). Although we do not propose additional interpretations of these flows beyond their connection with solitary waves, it may be of interest to mention here the original work developing the concept of conjugate columnar states, which had a more ambitious aim. Benjamin's (1962) theory of vortex breakdown suggested the pairing of a supercritical flow and its principal subcritical conjugate in analogy with shock jump conditions in gasdynamics, or hydraulic jumps in shallow-water theory. As Benjamin pointed out, a direct join of two solutions is not possible, since the members of the conjugate pair have different 'flow force' or axial momentum fluxes. If the differences in the flow forces of the conjugate columnar flows are small, Benjamin argued that the superposition of waves on the subcritical state can permit conservation of axial momentum. If the differences are too large, then energy loss is required to allow a momentum balance and the underlying assumptions are nullified. It is then difficult to imagine a physical interpretation yielding the principal conjugate as an end state. The same question might be raised in the weaker transition, where wave formation suffices to achieve a momentum balance, unless the transition region itself remains both steady and axisymmetric. It is worth noting, by way of concluding this discussion, that the BHE requires the specification only of $H'(\psi)$, not $H(\psi)$. Thus columnar conjugate states of the BHE can be joined, conserving mass, angular momentum, and axial momentum, by the loss of equal amount of total head on each streamline. This special form of energy loss leaves the BHE is unaltered. There is, however, no apparent reason why such a special arrangement of the energy loss should be realized.

4.2. *Numerical results*

Figure 1 is a bifurcation diagram for the columnar solutions branching from the primary flow (33), (34) with $\alpha = 14$, showing the principal and the second bifurcating branches. (The locations of the points of bifurcation are given in table 1 in §5.) The branches are described by a measure of the perturbation axial velocity. We took this to be the extreme value (regardless of sign), and on the principal bifurcating branch, on which the perturbation axial velocity is monotonic in r, this always occurred at the axis of rotation. On the second branch, the perturbation axial velocity is not monotonic. On this branch, a discontinuity appeared in the bifurcation diagram based upon the measure described: for a range of swirl parameter, the extreme value occurred on the axis, but shifted to a point off the axis, where the perturbation axial velocity was of opposite sign. This is illustrated by two sets of points in the figure, one as described, and the other (smooth) set arrived at by plotting only the perturbation axial velocity on the axis.

The supercritical portion of the principal columnar branch plays an important role, as will be seen in §5. By contrast, the physical significance of the second and higher columnar branches is unclear – for the larger amplitude perturbations on these branches, axial flow reversals are necessarily accompanied by internal zeros of the swirl, and hence instability according to the Rayleigh–Synge (1933) criterion (abbreviated subsequently to RS). This may be seen in figure 2, which shows profiles

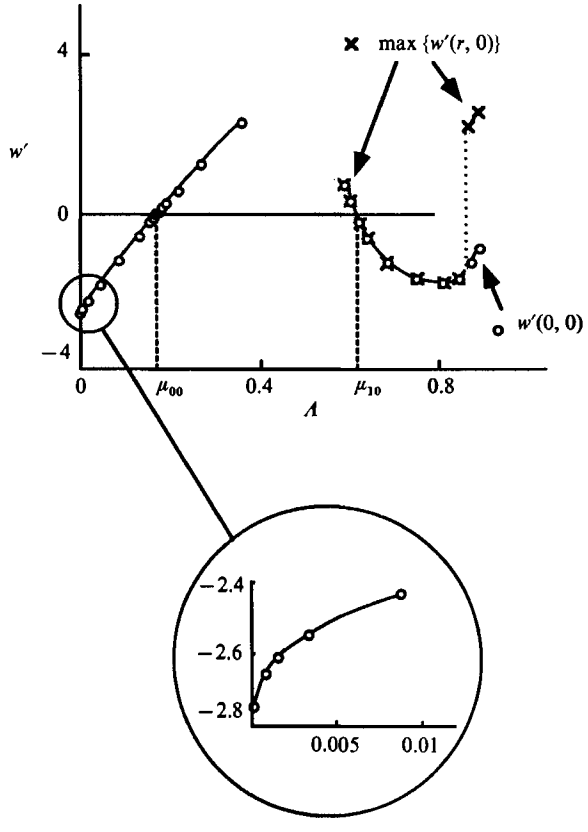

FIGURE 1. Bifurcation diagram for the first two columnar branches. The extreme perturbation axial velocity occurs away from the axis on part of the second branch.

from three points on the second branch of figure 1. Here the bifurcation point occurs at $\Lambda = \mu_{10}$, and the profiles are drawn for increasing values of Λ/μ_{10}. One can also see from the profiles for axial velocity how the discontinuity in the bifurcation diagram discussed in the previous paragraph arises. We shall not further discuss columnar branches other than the principal branch.

For $\Lambda < \mu_{00}$, the principal branch shows a developing wake-like axial velocity profile as the swirl parameter Λ is decreased from the branch point μ_{00}, as may be seen in figure 3. The swirl velocity is distorted as well, with the peak swirl moving outwards relative to that in the primary vortex. Both of these characteristics are qualitatively like the time-averaged profiles measured by Garg & Leibovich (1979) (further analysis of this data is given by L and by Leibovich 1978) *downstream* of vortex breakdowns, which are, like the solutions here, wake-like and subcritical. If Λ/μ_{00} is decreased below a value of about 0.5, the swirl velocity develops an internal zero, and the branch will become unstable according to the RS criterion. We have nevertheless continued to follow the branch, being curious to know if it could be continued to zero swirl, or whether it would turn around. We found that it *can* be continued to zero swirl, and the curvature of the magnified part of the bifurcation diagram of figure 1 indicates that the axial speeds get large as $\Lambda/\mu_{00} \to 0$. The axial profiles shown for $\Lambda/\mu_{00} = 0.001$ suggest that the limit flow becomes discontinuous, with a vortex sheet forming in the interior. The resolution of the singular limit

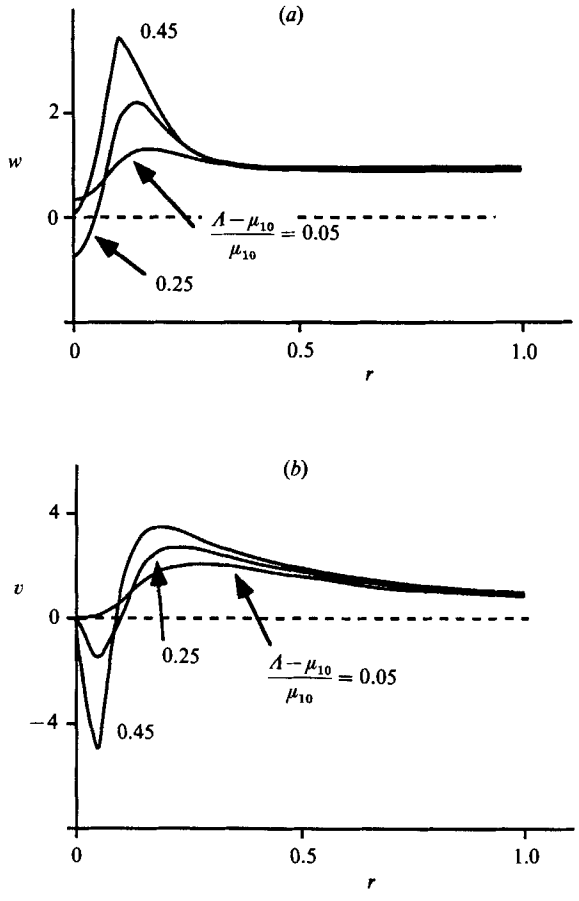

FIGURE 2. Velocities on the second columnar branch, for different values of the swirl parameter Λ. (*a*) Axial velocity, (*b*) azimuthal velocity.

behaviour as $\Lambda/\mu_{00} \to 0$ requires special treatment, and Appendix B is devoted to this question.

On the $\Lambda/\mu_{00} > 1$ side of the principal branch, the axial velocity profiles are jet-like, and the peak swirl moves towards the axis relative to that in the primary vortex. Examples are shown in figure 4. No tendency towards RS instability occurs on this side of the bifurcation point. These velocity profiles not only resemble the profiles measured by Faler & Leibovich (1977, 1978) and in the references cited in the previous paragraph for flows well *upstream* of vortex breakdown, they also can be accurately fitted, as can the wake-like solutions previously discussed, by the same exponential functions used in those references. We note further that the experimental data show the upstream flow to be not only jet-like, but supercritical. Thus, the primary vortex with uniform axial velocity generates, through its principal branch, vortices of the same character as those found on both upstream and downstream sides of experimentally observed vortex breakdowns, so far as the shapes of the profiles and their criticality conditions are concerned. It has already been noted in the Introduction, however, that one should recall that the jet-like flows here correspond to flows with different angular and axial momenta. They therefore cannot be identified with end states of a vortex breakdown flow in a constant-area tube

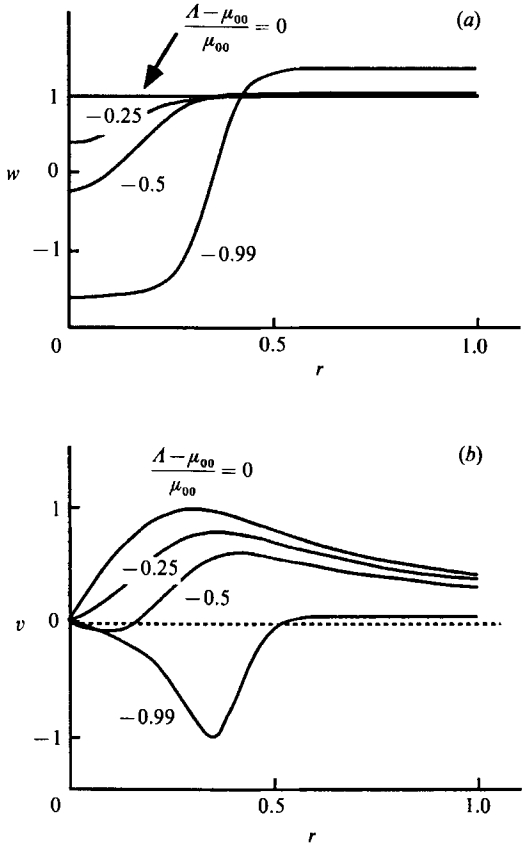

FIGURE 3. Velocities on the subcritical side of the principal columnar branch (supercritical conditions in the primary flow, $\Lambda < \mu_{00}$). (*a*) Axial velocity, (*b*) azimuthal velocity.

without invoking forces and torques outside the theory, a step which is not suggested here.

For $\Lambda < \mu_{00}$, the primary vortex is supercritical and the principal branch is subcritical, and according to the general theory of §4.1, these characteristics should be exchanged when $\Lambda > \mu_{00}$. We have tested this by computing the generalized Froude number, N, proposed by Benjamin (1962). This is defined to be

$$N \equiv \frac{c_+ + c_-}{c_+ - c_-},$$

where c_+ and c_- are, respectively, the maximum and minimum phase speeds of infinitesimal axisymmetric waves of extreme length propagating on the vortex. If $N > 1$, a vortex is supercritical, and if $N < 1$ it is subcritical. We have computed N on both the primary vortex and the principal branch, and the results, given in figure 5, confirm the general theory on exchange of criticality at the bifurcation point.

4.3. *Stability aspects*

Stability of the steady solutions treated here cannot be addressed using the BHE, since it contains no dynamics. Instead, one must return to the Euler equations. As a rule, vortex flows tend to less stable to non-axisymmetric perturbation than to

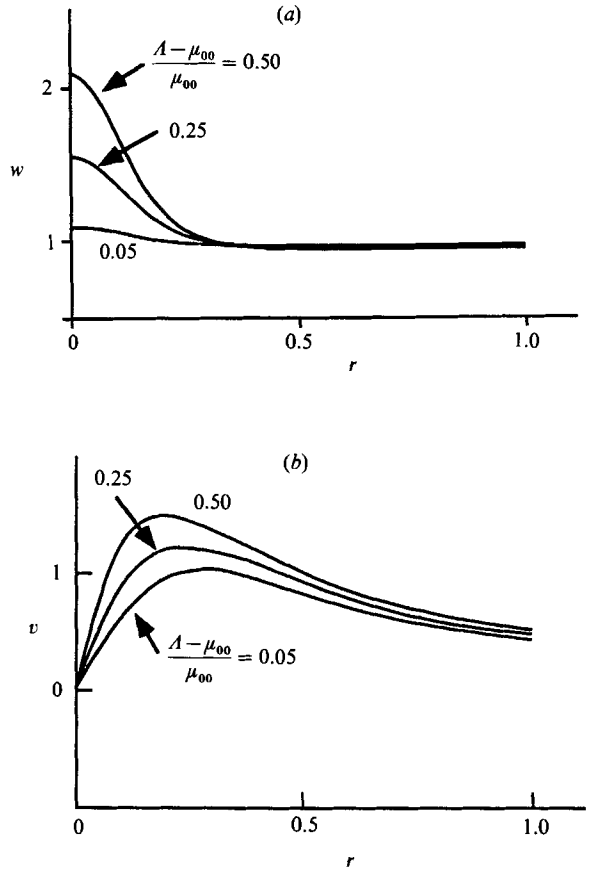

FIGURE 4. Velocities on the supercritical side of the principal columnar branch (subcritical conditions in the primary flow, $\Lambda > \mu_{00}$). (*a*) Axial velocity, (*b*) azimuthal velocity.

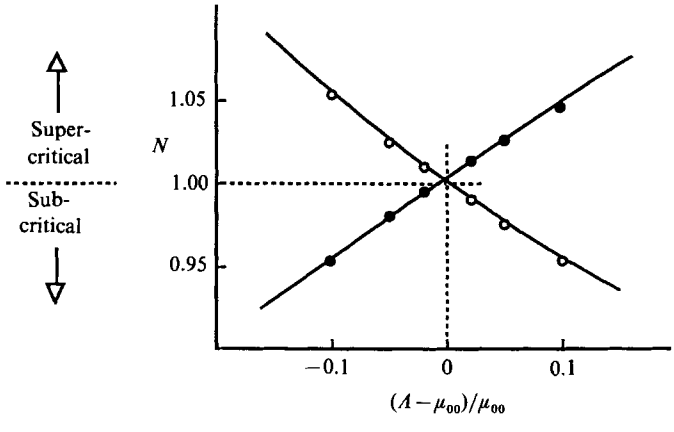

FIGURE 5. Exchange of criticality between the primary flow (—○—) and the principal conjugate branch (—●—), using Benjamin's Froude-number criterion.

axially symmetric ones. A bifurcation point is usually associated with a transfer of stability, so that in the present case, one would suppose that the specifying flow is stable and the principal branch is unstable on one side of the bifurcation point $\Lambda = \mu_{00}$, with the reverse being the case on the other side. This is assured if the eigenvalues of the temporal linearized stability problem, deriving from the Euler equations, are simple, and provided they move with a non-zero speed across the imaginary axis. In our example (33), at least when restricted to axisymmetric disturbances, the temporal eigenvalues are simple at the bifurcation points of the BHE equation, but bifurcation need not be associated with loss of stability, which implies that the temporal eigenvalues in such cases are confined to the imaginary axis. This may be seen from the axially symmetric Howard–Gupta equation (Howard & Gupta 1962), which governs the temporal stability problem. This equation is identical to (17*a*) provided only that the axial velocity of the specifying flow, $W(r)$, be replaced by $W(r)-c$, where $c = \omega/k$ is the (in general, complex) phase speed, and $\sigma = \mathrm{i}\omega$ is the temporal eigenvalue. In the example vortex (33), bifurcation does not lead to loss of stability. Here the Rayleigh discriminant is positive and there is no axial shear. Therefore, by Rayleigh's (1916) stability criterion, (33) is linearly stable to axisymmetric perturbations for all Λ. On the other hand, the same stability condition must hold for the solution branching from this point, at least for a limited range of Λ. This must be so since the linearized stability characteristics there are determined by the unperturbed flow at the bifurcation point, which is the same for all branches meeting there. Because the velocity profiles on the bifurcating branch deform continuously with Λ, there will be a finite Λ-interval over which the Richardson-number criterion of Howard & Gupta, which generalizes Rayleigh's criterion to admit axial shear, continues to guarantee linear stability to axially symmetric perturbations. The eigenvalues, σ, of the temporal stability problem can be found from the eigenvalues, μ, of the static bifurcation problem in the primary flow selected for numerical treatment (for which $W(r) = 1$), since it is easy to show that

$$\sigma = \mathrm{i}k\left[1 \pm \frac{\Lambda}{\mu}\right].$$

The eigenvalues σ are simple and lie on the imaginary axis for all Λ, and the zero eigenvalue is assumed when $\Lambda = \mu$.

Szeri (1988) has shown that, within the confines of the Arnol'd–Casimir theory, these results may be extended to weakly nonlinear stability. (This theory has been applied to axisymmetric swirling flow by Szeri & Holmes 1988. Its interpretation and significance is a complicated matter that requires and deserves further study.)

A simple test due to Leibovich & Stewartson (1983) exists by which one may determine if a columnar flow is unstable to non-axisymmetric perturbations. If this test is applied to the principal columnar branch displayed in figures 1 and 3, we find that instability to non-axisymmetric perturbations is indicated for $\Lambda/\mu_{00} < 0.88$ (recall the flow is wakelike for $\Lambda/\mu_{00} < 1$). The Howard–Gupta criterion is satisfied for $\Lambda/\mu_{00} > 0.6$, indicating that flows in this range are stable to axisymmetric perturbations. Neither test is useful where the corresponding inequality fails. To characterize the stability of these flows more completely requires stability calculations beyond the scope of the present paper.

α	L	μ_{00}	μ_{01}	μ_{10}
2	6	1.8433	1.9693	6.2743
	20	1.8433	1.8547	6.2743
14	6	0.17390	0.17986	0.61147
	20	0.17390	0.17445	0.61147
	100	0.17390	0.17392	0.61147

TABLE 1. Eigenvalues of the linearized problem for selected values of L and α

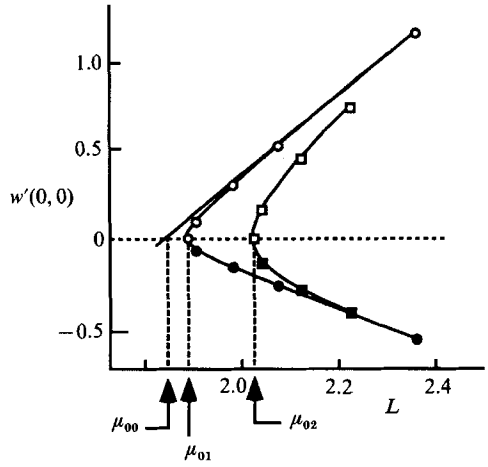

FIGURE 6. Bifurcation diagram for the periodic branches of μ_{01} and μ_{02}; $\alpha = 2$ for better separation of the bifurcation points. ——, principal columnar branch; —○—, $L = 10$, wave centred at $z = \frac{1}{2}L$; —●—, $L = 10$, wave centred at $z = 0$; —□—, $L = 5$, wave centred at $z = \frac{1}{2}L$; —■—, $L = 5$ wave centred at $z = 0$.

5. Periodic wavetrains

5.1. *Numerical results*

The specifying flow is subcritical for $\Lambda > \mu_{00}$: for any Λ in this range, an infinitesimal standing wave is possible, with wavelength depending on Λ. Fixing the wavelength at L, we continue infinitesimal standing waves to finite amplitude for the specifying flow (34) with $\alpha = 2$ and $\alpha = 14$ using the methods previously described. The larger value of α was used in an earlier study by Leibovich (1970), because it provided a good fit to Harvey's (1962) experimental data. The eigenvalues μ_{pm}, determined numerically as described in Appendix A, are given in table 1 for $\alpha = 2$, $L = 6$ and 20, and for $\alpha = 14$, $L = 6$, 20 and 100.

Figure 6 is the bifurcation diagram for the case $\alpha = 2$ and $L = 10$. The diagram for $\alpha = 14$ is qualitatively similar, but the separation between the curves for the columnar branch and the first wavy branch closes too rapidly to be conveniently illustrated in a drawing.

We next explore the waveform for three flows on the fundamental wavy branch for the case $\alpha = 14$. The stream function at a fixed value of $r = 0.25$ is plotted in figure 7 (*a*) as a function of z over one wavelength, for three values of Λ/μ_{00}. As Λ/μ_{00} increases, the wave trough becomes increasingly sharp and concentrated, and the

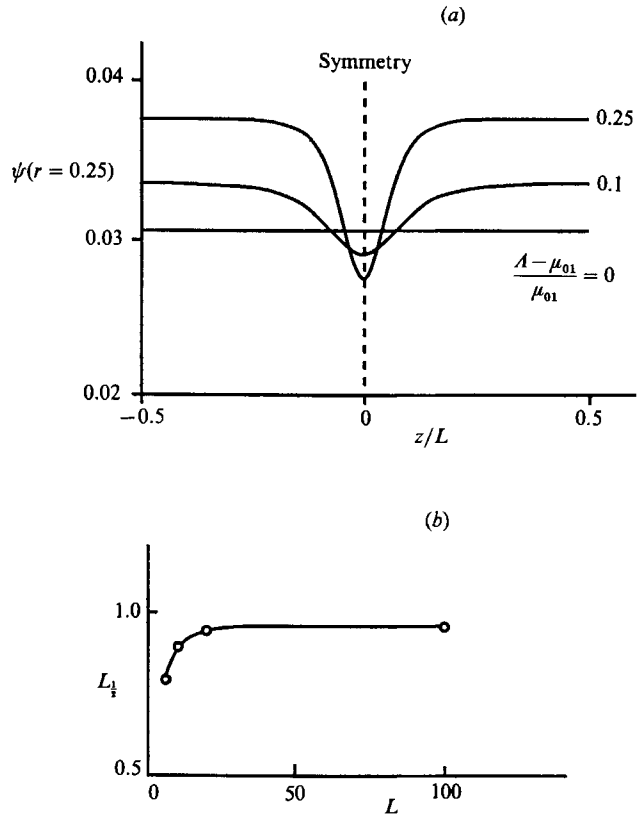

FIGURE 7. Approach of the periodic solutions to localized waves. (*a*) Fixed length $L = 6$: wave trough becomes localized as the wave amplitude increases. (*b*) Fixed amplitude $\Lambda/\mu = 1.10$: the half-height length of the wave approaches a constant value independent of the computational domain length.

wave crests increasingly broad and flat. The same trend is seen if the fundamental wavy branches for a sequence of flows of increasing wavelength L are sampled at fixed Λ/μ_{00} (figure 7*b*).

The changes in waveforms as either $(\Lambda - \mu_{00})/\mu_{00}$ or L increases are illustrated in figure 7. Increases in either of these parameters appear to produce a wave shape with a very sharp trough, in which there are strong axial accelerations, rapidly tending to a broad flat crest. Over most of its extent, this broad crest is an essentially columnar flow, but distorted considerably from the primary columnar flow. These features are characteristic of a solitary wave, with $L = \infty$, on a columnar flow different from the specifying flow.

Figure 8 shows streamlines projected onto a meridian plane for increasing values of Λ/μ_{00} for the case $L = 6$ and $\alpha = 14$. The deceleration of the upstream flow caused by the wave is apparent at the smallest value of Λ/μ_{00} shown. The other two streamline fields reveal a region of closed streamlines, with the size of the recirculation region growing with Λ/μ_{00}.

Velocity profiles at the wave trough are given in figure 9 (*a*, *b*) for a two swirl levels large enough to cause a region of reversed axial flow to appear. Figure 9 (*c*) shows the difference between the axial velocity at the trough and the axial velocity at the crest, where the flow is nearly columnar and, as will be shown, virtually indistinguishable

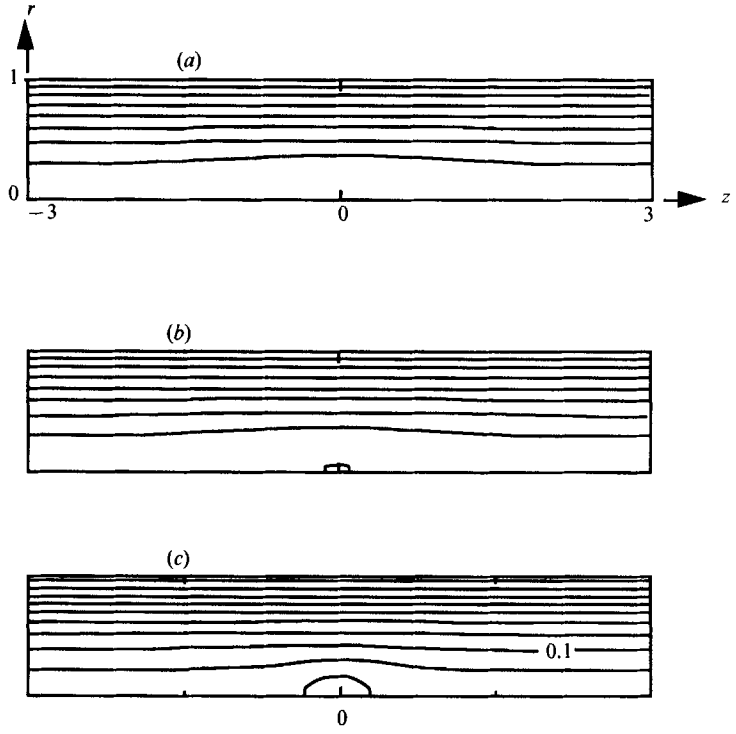

FIGURE 8. Meridional streamlines of periodic solutions; $L = 6$, $\alpha = 14$, contour intervals of 0.1. (*a*) $(\Lambda-\mu)/\mu = 1.5$, just before the appearance of stagnation points. (*b*) $(\Lambda-\mu)/\mu = 1.6$, a recirculation region grows with the perturbation amplitude.

from the principal conjugate flow. This is a perturbation which will be seen in figure 11 to be caused to the *principal conjugate flow* by the disturbance concentrated near the wave trough, rather than a perturbation to the specifying flow. The profiles in figure 9(*c*) are similar to the perturbation axial velocity in solitary waves on the specifying flow.

The observations we have made about the apparent appearance of solitary-wave behaviour will now be put to quantitative tests.

The characteristic length of a solitary wave can be measured by, say, its half-height length. According to the weakly nonlinear soliton solution (29), the half-height length (or any other measure of the solitary-wave length) scales with the inverse square root of the wave amplitude, $1/(\epsilon a)^{\frac{1}{2}}$, or alternatively, with $1/|\Lambda-\mu_{00}|^{\frac{1}{2}}$, at least for $|\Lambda-\mu_{00}|$ sufficiently small. The axial velocity perturbation at the origin is proportional to the wave amplitude, ϵa. In figure 10 we have plotted the half-height calculated from our numerically determined solutions on the first wavy branch for several wavelengths $L = (6, 20$ and $100)$, against the axial velocity perturbation at the origin to test whether the amplitude–length scaling appropriate to the weakly nonlinear solitary wave is approached by a wave of the computed periodic wavetrain. Waves exhibiting that scaling will have a slope of $-\frac{1}{2}$ on this log–log plot, and the solid line drawn has that slope. The wavetrain with period $L = 6$, given by the open circles, deviates substantially from the $-\frac{1}{2}$ slope both for small and large wave amplitude. The longer waves, however, accurately display the solitary-wave scaling for amplitudes ranging from fairly small values to quite substantial ones. Marked deviations from the weakly nonlinear solitary-wave scaling

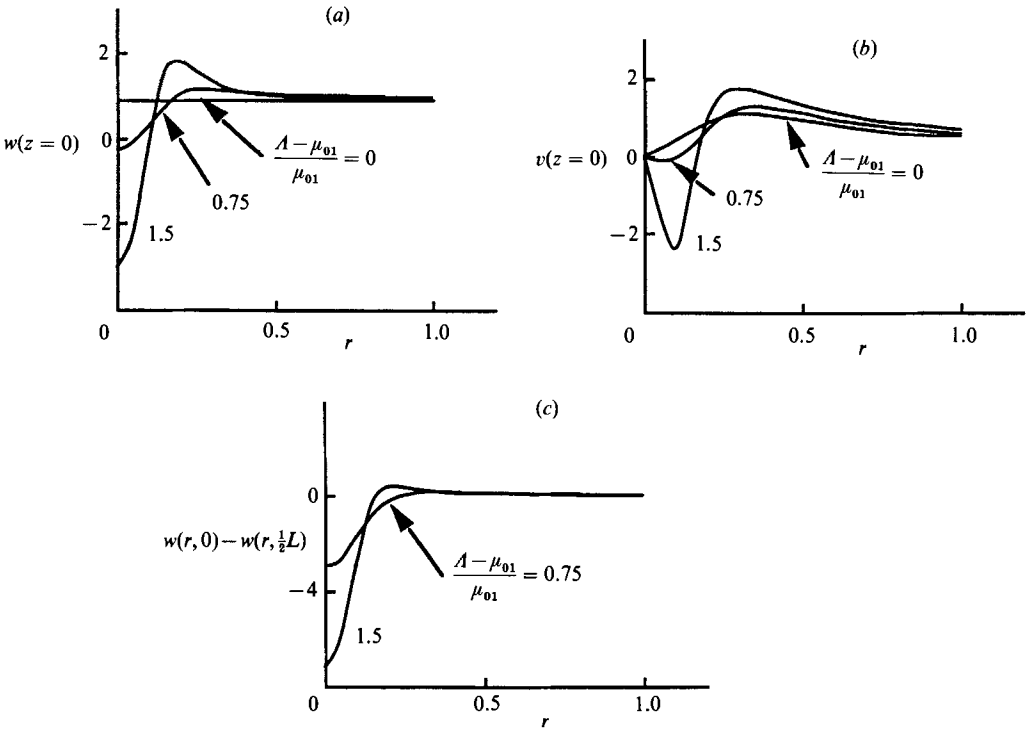

FIGURE 9. Velocities on the periodic branch of μ_{01} at the wave centre $z = 0$. (*a*) Axial velocity, (*b*) azimuthal velocity, (*c*) difference in axial velocity between the wave centre and tail.

occur for very small axial velocity perturbations and for axial velocity perturbations of $O(1)$ and higher. As will be seen in the next section, strong nonlinear effects distort the solitary wave on the primary flow in the same way, and begin to substantially modify the weakly nonlinear scaling at about the same level of axial velocity perturbation. These deviations from the weakly nonlinear scaling do not signal departures from solitary-wave behaviour, but rather transitions to a strongly nonlinear solitary-wave regime. We note that for large perturbations, the $L = 6$ case falls on the same curve as the longer waves, implying that the period of this wave is not long enough to exhibit solitary-wave behaviour at small amplitude, but that it does develop strongly nonlinear solitary-wave behaviour at large amplitude.

We conclude from these considerations that one wavelength of a periodic wavetrain rapidly approaches a solitary wave as the wave amplitude increases above a modest level. The resulting motion may be characterized either as weakly or as strongly nonlinear solitary waves, depending upon amplitude. Furthermore, the columnar flow to which these solitary waves tend, at distances from the station of maximum amplitude large compared to the half-length $L_{\frac{1}{2}}$, is not the specifying flow, but the principal conjugate flow. This point is illustrated in figure 11. Figure 11 (*a*) shows the difference between the stream function of the principal conjugate flow and that of the first wavy branch as a function of r for wavelength $L = 6$ for three values (0.05, 0.25, and 1.0) of $(\Lambda-\mu_{00})/\mu_{00}$, corresponding to waves of increasing amplitude. At the largest $(\Lambda-\mu_{00})/\mu_{00}$ (hence the largest amplitude), the difference is barely detectable. Figure 11 (*b*) shows the same tendency as L increases with the wave amplitude fixed.

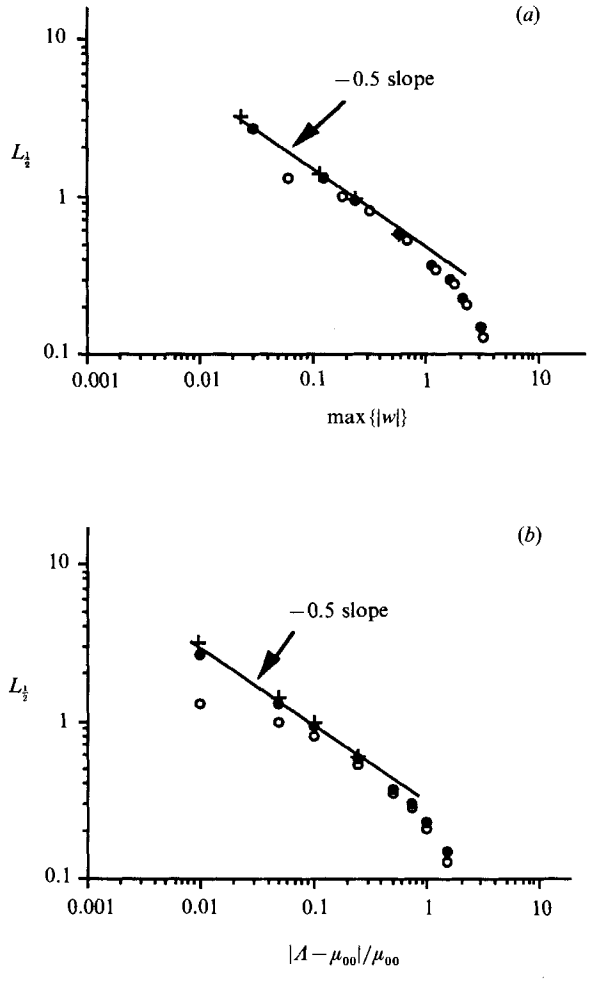

FIGURE 10. Solitary-wave behaviour of the periodic solutions: the dependence of effective wavelength (half-height length) on the wave amplitude, compared to the −0.5 slope for an exact solitary wave. ○, $L = 6$; ●, $L = 20$; +, $L = 100$. (*a*) Wave amplitude measured by extreme axial velocity, (*b*) wave amplitude measured by the distance from the bifurcation point.

5.2. *Closed streamlines and the Prandtl–Batchelor condition*

When stagnation points form, and with them recirculation regions of closed streamlines, we must reconsider the interpretation of the results. This is due to the well-known non-uniqueness of steady, axially symmetric, inviscid flows with closed streamlines. When closed streamsurfaces exist, the specification of the vorticity distribution by functional forms for $H'(\psi)$ and $F(\psi)$ determined by the upstream flow need not be continued into the region of closed streamlines. In fact, if the flow is to be perfectly steady and either two-dimensional or axially symmetric, and to be the limit of a viscous flow as the viscosity vanishes, the vorticity in the recirculation region must satisfy the constraints found by Prandtl (1904) and Batchelor (1956). For axisymmetric flow this requires $F(\psi) \equiv 0$ and $H'(\psi) =$ constant ($= h_p$, say). One might think that a solution with closed streamlines, ignoring the Prandtl–Batchelor (or PB) condition, can be made consistent with it by recomputing the flow inside the

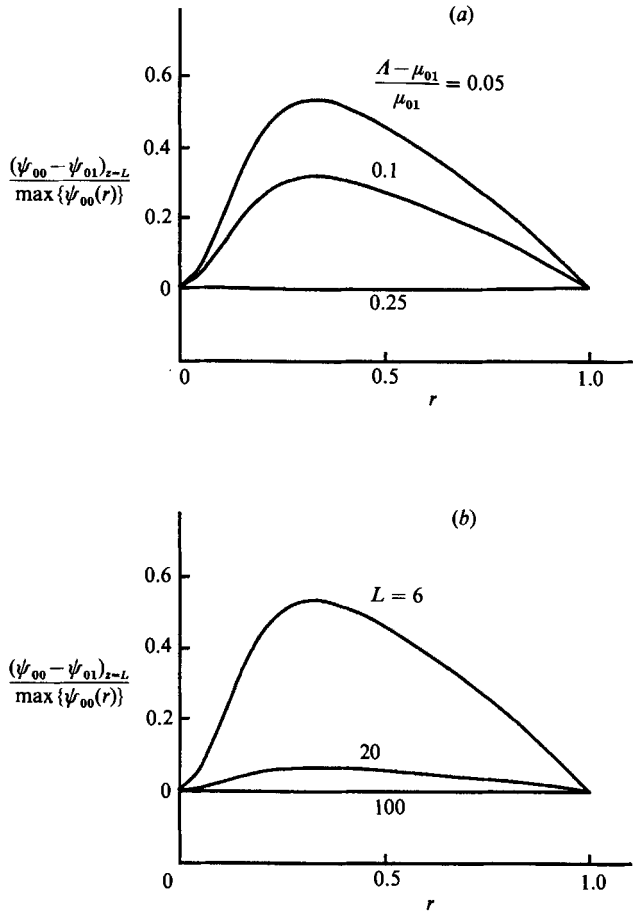

FIGURE 11. Convergence of the wave crests of the periodic solution to the columnar solution of the same amplitude. (*a*) Fixed length $L = 6$, the difference vanishes as the wave amplitude increases. (*b*) Fixed amplitude $(\Lambda-\mu_{01})/\mu_{01} = 0.05$, as the computational domain length increases.

dividing streamsurface, using the PB criterion to fix the interior vorticity distribution, but maintaining the exterior flow and the shape of the dividing streamsurface. This generally cannot be done, however, while balancing the interior and exterior pressures. Thus, if the PB condition is invoked, flows computed with an arbitrary specifying flow upstream and containing closed streamlines must be replaced by solutions of a free streamline type of problem, in which the boundary shape between the external region (specified by upstream conditions) and the internal region (PB flow) is part of the problem (see Leibovich 1968 for an example of such a construction).

The wavetrains of §5.1 do not exhibit closed streamlines for $\Lambda/\mu_{01} < 2.5$, and in this range the indeterminacy in F and H does not arise. At the upper end of this range of Λ/μ_{01}, the waves are highly nonlinear. For larger values of Λ/μ_{01}, the indeterminacy arises. A similar indeterminacy arises in those columnar flows discussed in §4 containing lines with zero axial velocity. Passing through this line implies that the stream function *vs.* radius relationship cannot be inverted as done in §2. Non-uniqueness follows, and different functional forms for F and H may be

postulated on either side of the line where $w = 0$. Here there are no closed streamlines, except perhaps in a limiting sense, where streamlines close 'at infinity'.

One way to resolve the indeterminacy is to invoke the PB condition (in addition, a matching between the interior and exterior flows is required to fix h_p.) On the other hand, the PB condition is not a fundamental physical principle: Batchelor (1956) points out circumstances in which it is not applicable even when the flow is precisely steady and axisymmetric. The PB condition is based on the achievement of a double limit, $t \to \infty$, $\nu \to 0$, while maintaining two-dimensional or axisymmetric symmetry; this is done (Batchelor 1956) by considering steady, symmetric flows with a decreasing but non-zero viscosity. One must, then, consider questions of the timescales and the robustness of symmetry before applying the PB condition to any specific problem.

The PB condition is not relevant if the flow is not exactly axisymmetric, even if the non-axisymmetric component of the flow is weak, since there is then fluid exchange across the nominal closed streamsurface. Our view of vortex breakdown leads us to contemplate flows in which symmetry-breaking instability is active. The present steady, axisymmetric solutions are expected to serve as a component in a composite model which includes additional contributions (effects (2) and (3) as presented in the Introduction.) With this view of the overall flow structure, the vorticity distribution inside closed streamlines need not be constrained by the PB condition. We have chosen to continue smoothly the functional form of $H'(\psi), F(\psi)$ from the region outside the closed streamlines. If a small non-axisymmetric component is present with an axisymmetric recirculation zone, the fluid exchange across (at least a portion of) the nominal boundary would, in our view, create an interior vorticity distribution that is not inconsistent with that in the external flow. Thus, in an average sense, the functional form of $H'(\psi), F(\psi)$ should vary smoothly across the boundary of the recirculation zone. A reasonable form for the circulation in the interior would be $-F(\psi)$, not $F(\psi)$, to produce a flow with an interior swirl sense in agreement with that in the external flow, which is certainly required if there is exchange of fluid; this alteration is dynamically compatible with the flows computed here (as pointed out in L). Thus, it is our view that the flows calculated here having recirculation regions are sensible, although possibly too simplistic, models of real vortex flows with stagnation points and a semblance of an axisymmetric recirculation region (albeit a broken one). We are in the process of exploring the breaking of the symmetry of the flows produced in this paper, and intend to report on that investigation in the future.

6. Solitary waves on the specifying flow

When the specifying flow is slightly supercritical, a weakly nonlinear solitary wave (29*a*) is possibie. A diagram summarizing the numerical continuation of this solitary wave solution branch to more strongly supercritical conditions (Λ decreasing from μ_{00}; note that the scaled distance from the branch point, $|\Lambda - \mu_{00}|/\mu_{00}$, ranges from zero to a maximum of unity) is given in figure 12. The diagram superposes two measures of the wave disturbance of the specifying columnar flow, the maximum perturbation axial velocity ($w'_{\max}$) at the plane of symmetry $z = 0$, and the perturbation axial velocity on the axis at this plane ($w'(0,0)$). The two measures agree for values of $|\Lambda - \mu_{00}|/\mu_{00}$ as large as 0.8. For larger values of this parameter, the point at which the perturbation axial velocity is a maximum lifts off of the rotation axis.

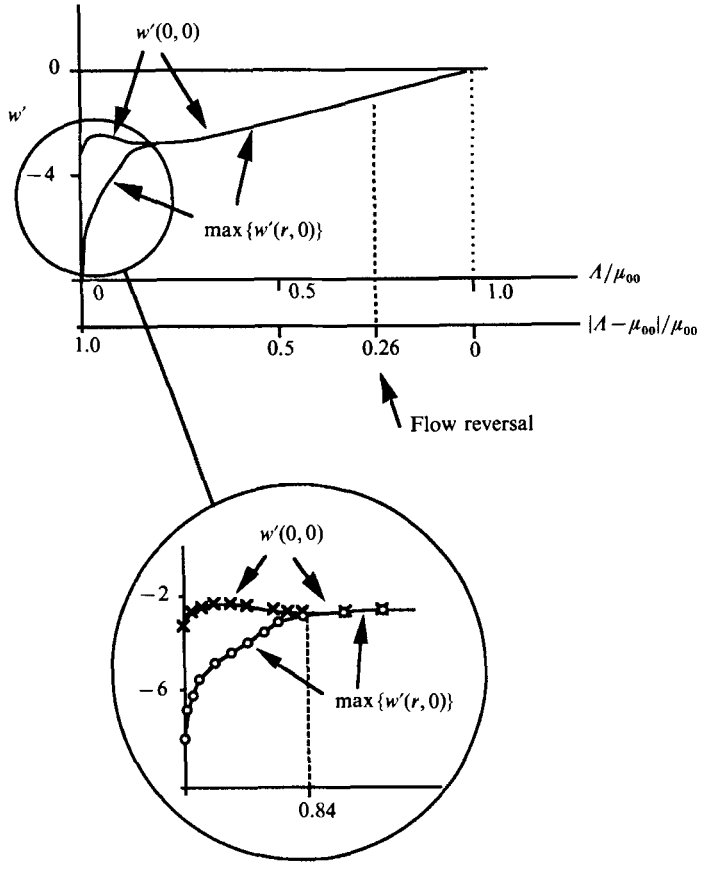

FIGURE 12. Bifurcation diagram, solitary wave branch. The extreme perturbation axial velocity is off the axis when $\Lambda < 0.16\mu_{00}$.

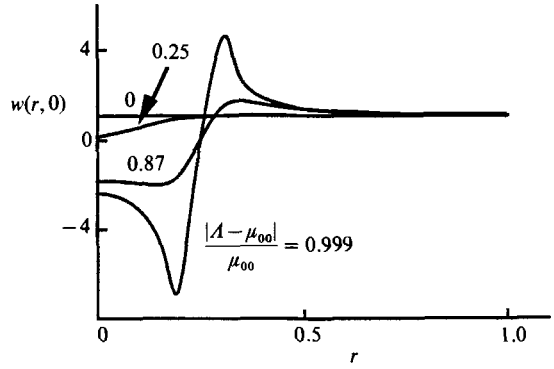

FIGURE 13. Axial velocity at wave centre $z = 0$ on the solitary-wave branch.

The shift of the point of maximum axial velocity disturbance may also be seen in the axial velocity profiles at the symmetry plane. Profiles of the complete axial velocity component are drawn in figure 13 for four values of Λ. Three of the profiles include negative values of w, which implies the existence of a region of closed streamlines containing reversed axial velocities. The discussion in §5.2 applies to the

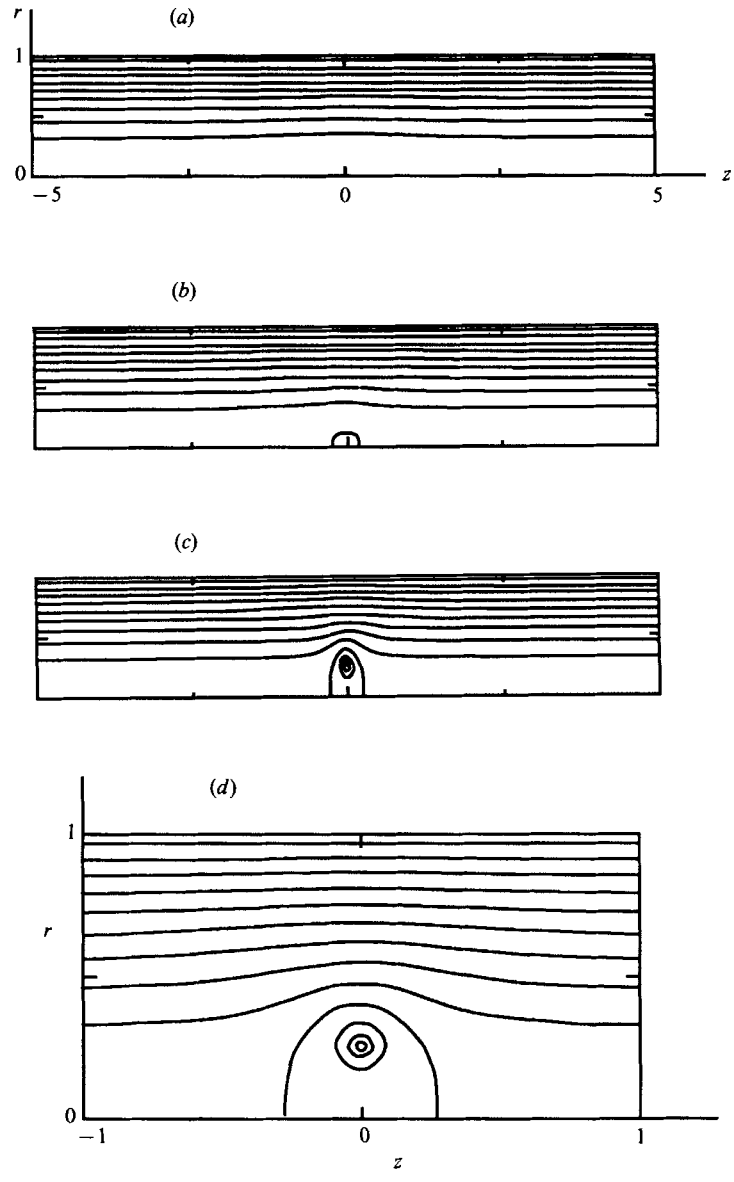

FIGURE 14. Meridional streamlines of solitary-wave solutions, $L = 10$, contour intervals 0.05. (*a*) $A/\mu_{00} = 0.80$, (*b*) $A/\mu_{00} = 0.70$, a small recirculation bubble appears, (*c*) $A/\mu_{00} = 0.001$, a large recirculation bubble. (*d*) Detail of the bubble in (*c*).

part of this branch exhibiting closed streamlines ($A < 0.74\mu_{00}$). When the maximum perturbation lifts off the axis, a high-speed upstream-directed jet forms in the interior of the recirculation region, and the dividing streamline develops a dimple at the axis and is no longer convex. We are unaware of observations of such a phenomenon, and believe it to be physically unrealizable.

Projections of the streamlines onto the meridian plane are shown in figure 14. These plots show the emergence of the recirculation region. We have found that the flow field is represented with reasonable accuracy by the weakly nonlinear solution

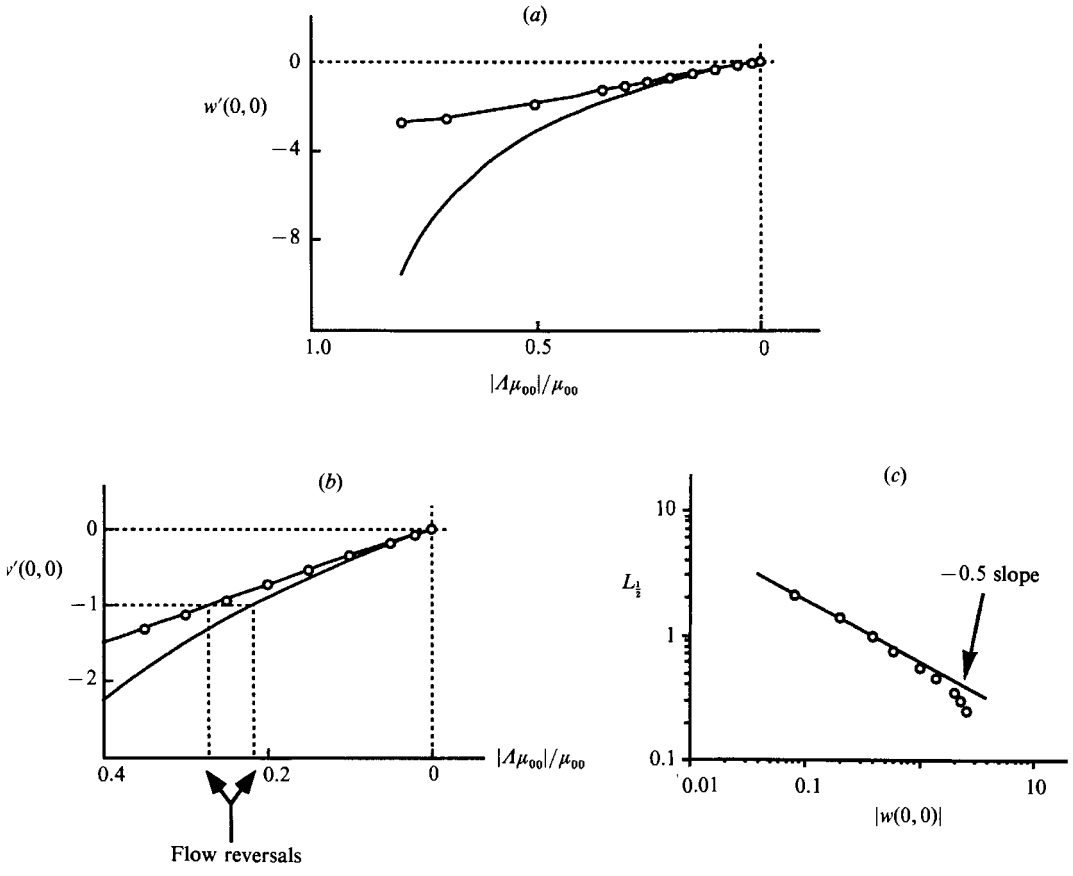

FIGURE 15. Comparison of solitary-wave amplitude of the computed (○) and weakly nonlinear (——) solutions. (*a*) Bifurcation diagram, (*b*) detail showing the bifurcation and the amplitudes of flow reversal. (*c*) Half-height length *vs.* amplitude of the computed wave, compared to the −0.5 slope of the exact solitary wave.

(29*a*) for waves leading to axial velocity perturbations strong enough to cause flow reversal. This is a significant finding, since we may then capture the essentials of our numerical computations of a strongly perturbed flow with the simple formula (29). To show the level of agreement, we have compared (for $\alpha = 14$) $w'(0,0)$ from our numerical computations with the approximation (29*a*). This is found in figure 15, together with a comparison of the dependence of wave half-length on wave amplitude (measured by $w'(0,0)$) compared to the $-\frac{1}{2}$ power-law dependence obeyed by the weakly nonlinear solitary wave. The weakly nonlinear solution (29*a*) overpredicts the wave amplitude and length, but the differences are less than 10% for wave amplitudes large enough to cause stagnation and reversed axial flow.

Contours of the perturbation stream functions, as predicted by numerical computation and by the weakly nonlinear approximation (29*a*), are shown in figure 16. We judge the agreement to be qualititatively good for all three values of $|\Lambda-\mu_{00}|/\mu_{00}$ shown, quantitatively good for $|\Lambda-\mu_{00}|/\mu_{00} = 0.1$, and acceptable for some purposes for the higher values of $|\Lambda-\mu_{00}|/\mu_{00}$. It is worth noting that a stagnation point first appears in the flow for $|\Lambda-\mu_{00}|/\mu_{00} \approx 0.25$, so the three cases shown in figure 15 range from moderately to strongly nonlinear.

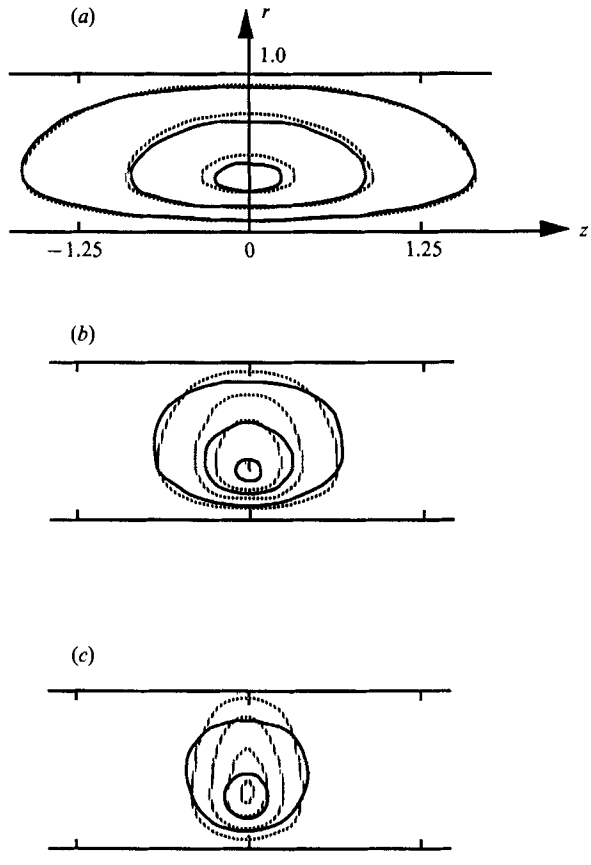

FIGURE 16. Comparison of perturbation streamlines of the computed (——) *vs.* the weakly nonlinear (· · · · · ·) solitary waves. (*a*) $\Lambda/\mu_{00} = 0.90$, contour intervals 0.004, (*b*) $\Lambda/\mu_{00} = 0.50$, contour intervals 0.012, (*c*) $\Lambda/\mu_{00} = 0.20$, contour intervals 0.02.

7. Discussion and conclusions

We have shown here the relationships between fully nonlinear standing periodic wavetrains and solitary waves and the underlying columnar flows. From a given primary, or 'specifying', columnar flow, other columnar flows, solitary waves, and periodic wavetrains may be constructed. Of the additional possible columnar flow branches, the one we have designated the 'principal conjugate' is of special interest. It branches from the primary flow at the critical swirl level, and has been shown to be supercritical when the primary flow is subcritical, and vice versa.

Solitary waves exist only when the primary flow is supercritical, a condition that arises when the swirl rate of axial vorticity in the primary flow is less than an easily determined critical value. Periodic wavetrains exist only when the primary flow is subcritical, which arises when the swirl rate exceeds the critical value. On the other hand, the periodic wavetrains rapidly attain the characteristics of solitary waves as the swirl, and with it the wave amplitude, increase for fixed wavelength; or as the wavelength increases at fixed, but finite, amplitude. These can be interpreted as solitary waves propagating on the principal conjugate flow in the range where it is

supercritical. Thus the requirement that flow upstream of solitary waves must be supercritical is maintained.

The simple, partly analytical, formula for weakly nonlinear solitary waves is shown to fit the numerical data for fully nonlinear solitary waves very well for a substantial range of amplitudes. The errors associated with this fit are relatively small even for waves with amplitudes large enought to cause stagnation points and reversed axial flow to occur.

The phenomenon of vortex breakdown supplies us with the main motivation for the present study of large-amplitude waves, but other applications exist. These waves can propagate on vortex cores without reaching amplitudes extreme enough to cause recirculation to occur, and must be presumed a possibility on a wide variety of concentrated vortex flows. We have outlined in the paper a hypothesis in which the large waves serve as one of the building blocks in a theoretical proposal for vortex breakdowns. We are presently exploring complementary aspects of this proposal.

We have benefitted from comments and suggestions made by Professor T. Brooke Benjamin for which we are grateful. This work was supported by the US Air Force Office of Scientific Research under grants AFOSR-87-0255 and AFOSR-89-0346, monitored by Dr L. Sakell. Additional support was provided by the grant AFOSR-89-0226, monitored by Dr J. McMichael, and by the US Army Research Office at the Mathematical Sciences Institute of Cornell University.

Appendix A. Numerical implementation

A.1. *Discretization*

A finite-difference discretization is done on equation (16), written in the form:

$$\mathrm{D}^2\Phi+\Omega(\Phi,r;\Lambda)=r\frac{\partial}{\partial r}\left(\frac{1}{r}\frac{\partial\Phi}{\partial r}\right)+\frac{\partial^2\Phi}{\partial z^2}+\Omega(\Phi,r;\Lambda)=0. \tag{A 1}$$

The finite-difference approximation corresponding to this form of the radial derivatives has the property that the contribution of each cell boundary to the circulation around the cell is the same for the two cells adjacent at that boundary; the result is that any group of cells satisfy the Stokes theorem when individual cells do, similar to the flux consistency in 'conservative' discretization of the Navier–Stokes or the energy equation.

We expect solutions that have sharp axial gradients, and non-uniform grid spacing may be necessary in the z-direction. This is done by defining a computational coordinate ζ, related to the physical coordinate z by $z=f(\zeta)$ $(f'(\zeta)\neq 0)$; the z-derivative in (A 1) becomes

$$\frac{\partial^2\Phi}{\partial^2 z}=\frac{1}{f'(\zeta)}\frac{\partial}{\partial\zeta}\left(\frac{1}{f'(\zeta)}\frac{\partial\Phi}{\partial\zeta}\right).$$

Equation (A 1) is discretized by central differences on a rectangular grid having uniform spacing in (r,ζ), corresponding to variable spacing in z. The finite-dimensional version of (A 1) is

$$\mathbf{D}\Phi+\boldsymbol{\Omega}(\Phi,\Lambda)=0, \tag{A 2}$$

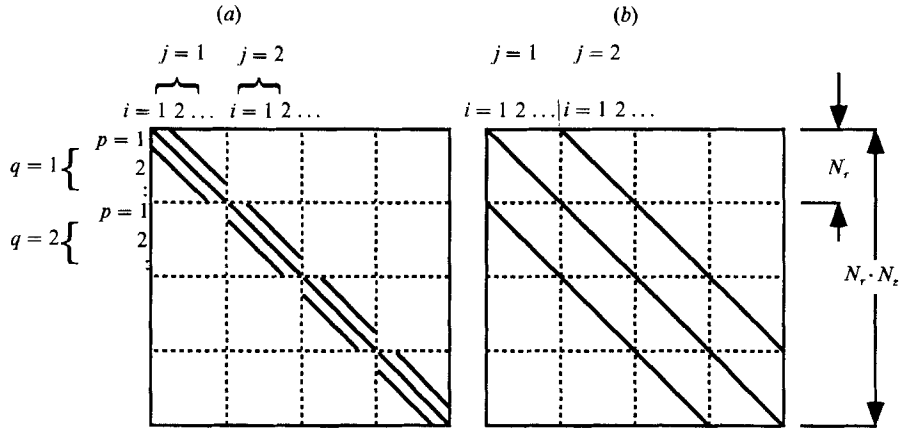

FIGURE 17. Structure of the matrices (a) $\mathbf{D}^r_{pqij}$, (b) $\mathbf{D}^z_{pqij}$.

where

$$(\boldsymbol{\Phi})_{ij} \equiv \Phi(r_i, \zeta_j),$$

$$(\boldsymbol{\Omega})_{ij} \equiv \Lambda(\boldsymbol{P})_{ij} + (\boldsymbol{Q})_{ij} \equiv \Lambda P((\boldsymbol{\Phi})_{ij}) - r_i^2 Q((\boldsymbol{\Phi})_{ij}),$$

$$\mathbf{D} \equiv \mathbf{D}^r + \mathbf{D}^z,$$

$$(\mathbf{D}^r)_{pqij} = \begin{cases} \Delta r^{-2}\left(1 - \dfrac{\Delta r}{2r_p}\right)^{-1}, & j = q \text{ and } i = p-1, \\ -2\Delta r^{-2}\left(1 - \left(\dfrac{\Delta r}{2r_p}\right)^2\right)^{-1}, & j = q \text{ and } i = p, \\ \Delta r^{-2}\left(1 + \dfrac{\Delta r}{2r_p}\right)^{-1}, & j = q \text{ and } i = p+1, \\ 0, & \text{otherwise}; \end{cases}$$

$$(\mathbf{D}^z)_{pqij} = \begin{cases} \Delta\zeta^{-2}[f'(\zeta_q)f'(\zeta_q - \Delta\zeta/2)]^{-1}, & i = p \text{ and } j = q-1, \\ -\Delta\zeta^{-2}f'(\zeta_q)^{-1}[f'(\zeta_q + \Delta\zeta/2)^{-1} + f'(\zeta_q - \Delta\zeta/2)^{-1}], & i = p \text{ and } j = q, \\ \Delta\zeta^{-2}[f'(\zeta_q)f'(\zeta_q + \Delta\zeta/2)]^{-1}, & i = p \text{ and } j = q+1, \\ 0, & \text{otherwise.} \end{cases}$$

$\mathbf{D}^r$, $\mathbf{D}^z$ are 'directional operators', containing entries relevant to the derivatives in r, ζ-directions. Each contains three non-zero diagonals in block structure as shown in figure 17. The separation of $\mathbf{D}$ into its directional components and the structure of these components will be used in §A 2 below to form efficient and consistent concepts of separation of variations and inner product for the discrete problem (A 2).

The contribution of boundary points with Dirichlet-type boundary conditions is placed in $\boldsymbol{\Omega}$ when non-zero; for Neumann-type boundary conditions, an external node is defined outside the boundary, its value given by the first derivative at the boundary; for $\mathrm{d}\Phi/\mathrm{d}n = 0$, we set $\Phi_{B+1} = \Phi_{B-1}$ in the equation for the boundary node Φ_B. The singularity of (A 1) at $r = 0$ is not explicitly present in the numerical problem, since $\Phi = 0$ at $r = 0$, and the discretization of (A 1) takes place only in the interior of the domain – a finite distance from $r = 0$ (more on this singularity in §A 4).

A.2. *Algebraic treatment of the bifurcation and continuation*

In the neighbourhood of any bifurcation point $\Lambda = \mu$, we expand the solution to (A 2) in a small parameter ϵ, as in (18):

$$\boldsymbol{\Phi} = \epsilon\boldsymbol{\phi}_0 + \epsilon^2\boldsymbol{\phi}_1 + \ldots, \quad \Lambda = \mu + \epsilon\kappa_0 + \epsilon^2\kappa_1 + \ldots. \tag{A 3}$$

Substituting into (A 2) and collecting terms of like power in ϵ, we obtain the sequence of equations, analogous to (20), the first three of which are

$$\mathbf{L}\boldsymbol{\phi}_0 \equiv [\mathbf{D} + \mu\boldsymbol{P}^{(1)} + \boldsymbol{Q}^{(1)}]\boldsymbol{\phi}_0 = [\mathbf{D} + \boldsymbol{S}^{(1)}]\boldsymbol{\phi}_0 = 0, \tag{A 4a}$$

$$\mathbf{L}\boldsymbol{\phi}_1 = -\kappa_0 \boldsymbol{P}^{(1)}\boldsymbol{\phi}_0 - \boldsymbol{S}^{(2)}\boldsymbol{\phi}_0\boldsymbol{\phi}_0, \tag{A 4b}$$

$$\mathbf{L}\boldsymbol{\phi}_2 = -\kappa_1 \boldsymbol{P}^{(1)}\boldsymbol{\phi}_0 - \kappa_0 \boldsymbol{P}^{(1)}\boldsymbol{\phi}_1 - 2\boldsymbol{S}^{(2)}\boldsymbol{\phi}_0\boldsymbol{\phi}_1 - \boldsymbol{S}^{(3)}\boldsymbol{\phi}_0\boldsymbol{\phi}_0\boldsymbol{\phi}_0 - \kappa_0 \boldsymbol{P}^{(2)}\boldsymbol{\phi}_0\boldsymbol{\phi}_0, \tag{A 4c}$$

where the derivatives of $\boldsymbol{\Omega}$ are defined following (19):

$$(\boldsymbol{P}^{(1)})_{pqij} = \frac{\partial(\boldsymbol{P})_{pq}}{\partial(\boldsymbol{\Phi})_{ij}}(\boldsymbol{\Phi} = 0), \quad (\boldsymbol{P}^{(2)})_{pqijkl} = \frac{\partial^2(\boldsymbol{P})_{pq}}{\partial(\boldsymbol{\Phi})_{ij}\partial(\boldsymbol{\Phi})_{kl}}(\boldsymbol{\Phi} = 0), \ldots,$$

$$(\boldsymbol{Q}^{(1)})_{pqij} = \frac{\partial(\boldsymbol{Q})_{pq}}{\partial(\boldsymbol{\Phi})_{ij}}(\boldsymbol{\Phi} = 0), \quad (\boldsymbol{Q}^{(2)})_{pqijkl} = \frac{\partial^2(\boldsymbol{Q})_{pq}}{\partial(\boldsymbol{\Phi})_{ij}\partial(\boldsymbol{\Phi})_{kl}}(\boldsymbol{\Phi} = 0), \ldots,$$

$$\boldsymbol{S}^{(k)} \equiv \mu\boldsymbol{P}^{(k)} + \boldsymbol{Q}^{(k)}.$$

The eigenvalue problem (A 4*a*) can be solved by separation of variables: let $\boldsymbol{\phi}_0$ have the form, equivalent to (21)

$$(\boldsymbol{\phi}_0)_{ij} = (\boldsymbol{\phi}_0^r)_i\,(\boldsymbol{\phi}_0^z)_j,$$

where $\boldsymbol{\phi}_0^r$ and $\boldsymbol{\phi}_0^z$ may be called 'directional' components of $\boldsymbol{\phi}_0$. Substituting into (A 4*a*) and using the repeated block structure of $\mathbf{D}$ we obtain

$$\{[(\mathbf{D}^r)_{p1i1} + \mu(\boldsymbol{P}^{(1)})_{p1i1} + (\boldsymbol{Q}^{(1)})_{p1i1}]\,(\boldsymbol{\phi}_0^r)_i\}\,(\boldsymbol{\phi}_0^z)_q = -(\boldsymbol{\phi}_0^r)_p\,\{(\mathbf{D}^z)_{1q1j}\,(\boldsymbol{\phi}_0^z)_j\}$$

which is an equality of two rank-1 matrices; there exists therefore a scalar β such that

$$-\beta(\boldsymbol{\phi}_0^z)_q + (\mathbf{D}^z)_{1q1j}\,(\boldsymbol{\phi}_0^z)_j = 0 \tag{A 5a}$$

and

$$(\boldsymbol{P}^{(1)})^{-1}_{k1p1}[(\mathbf{D}^r)_{p1i1} + \beta\boldsymbol{I}_{p1i1} + (\boldsymbol{Q}^{(1)})_{p1i1}]\,(\boldsymbol{\phi}_0^r)_i + \mu(\boldsymbol{\phi}_0^r)_k = 0. \tag{A 5b}$$

Note that $\boldsymbol{P}^{(1)}$ is invertible since it is a diagonal matrix having $p(r_i)$ entries on its diagonal, which are positive.

The eigenvalues β_n, μ_{nm} and their eigenvectors are found from (A 5) by the tridiagonal set of subroutines from EISPACK (Smith *et al.* 1976).

Define an inner product as follows:

$$\langle \boldsymbol{x}, \boldsymbol{y} \rangle = \boldsymbol{x}^{\mathrm{T}}\boldsymbol{S}\boldsymbol{y}, \tag{A 6}$$

where

$$(\boldsymbol{S})_{pqij} = (\boldsymbol{S}^r)_{pi}\,(\boldsymbol{S}^z)_{qj}$$

and $\boldsymbol{S}^r, \boldsymbol{S}^z$ are diagonal: $\boldsymbol{S}^r = \mathrm{diag}\,[p(r_i)/r_i]$, $\boldsymbol{S}^z = \mathrm{diag}\,[f'(\zeta_j)]$ (the first and last elements may be different owing to the boundary conditions); both are positive definite. Under this inner product, $(\boldsymbol{P}^{(1)})^{-1}\mathbf{L}$ is self-adjoint and the eigenvectors of (A 4*a*) are orthogonal.

Multiply (A 4*b*) by $(\boldsymbol{P}^{(1)})^{-1}$ to obtain the self-adjoint form of the operator, and we can impose a solvability condition:

$$\langle (\boldsymbol{P}^{(1)})^{-1}[\boldsymbol{S}^{(2)}\boldsymbol{\phi}_0\boldsymbol{\phi}_0 + \kappa_0 \boldsymbol{P}^{(1)}\boldsymbol{\phi}_0], \boldsymbol{\phi}_0 \rangle = 0. \tag{A 7}$$

This is used to find κ_0, as in (23). To solve (A 4*b*) for $\boldsymbol{\phi}_1$, we use an eigenvector expansion method. Similarly, κ_1 and $\boldsymbol{\phi}_2$ can be found from (A 4*c*), and so to any desired order. We used two or three terms of (A 3), depending on the type of bifurcation encountered.

Let $\dot{\boldsymbol{\Phi}} \equiv \partial\boldsymbol{\Phi}/\partial\Lambda$, and take the derivative of (A 2) with respect to Λ:

$$\mathbf{L}\dot{\boldsymbol{\Phi}} = -\boldsymbol{P}(\boldsymbol{\Phi}). \tag{A 8}$$

This is a system of ODE's for $\boldsymbol{\Phi}(\Lambda)$, equivalent to (29*b*); given initial conditions $\boldsymbol{\Phi}(\Lambda_0)$ from (A 3) or the weakly nonlinear estimate (30), this linear system can be solved for $\dot{\boldsymbol{\Phi}}$. We use SPARSPAK (George *et al.* 1980) to solve (A 8) and a Runge–Kutta integrator (Press *et al.* 1986) to integrate over Λ.

Given $\boldsymbol{\Phi}_0$ and Λ, an approximate solution of (A 2), we may define a Newton's method iteration (Dennis & Schnabel 1983):

$$\boldsymbol{\Phi}_{k+1} = \boldsymbol{\Phi}_k - [\mathbf{D} + \Lambda \boldsymbol{P}_k^{(1)} + \boldsymbol{Q}_k^{(1)}]^{-1}[\mathbf{D}\boldsymbol{\Phi}_k + \boldsymbol{\Omega}(\boldsymbol{\Phi}_k, \Lambda)], \tag{A 9}$$

where $$(\boldsymbol{P}_k^{(1)})_{pqij} = \frac{\partial(\boldsymbol{P})_{pq}}{\partial(\boldsymbol{\Phi})_{ij}}(\boldsymbol{\Phi} = \boldsymbol{\Phi}_k), \quad (\boldsymbol{Q}_k^{(1)})_{pqij} = \frac{\partial(\boldsymbol{Q})_{pq}}{\partial(\boldsymbol{\Phi})_{ij}}(\boldsymbol{\Phi} = \boldsymbol{\Phi}_k).$$

Under some mild assumptions, in particular that $\boldsymbol{\Phi}_0$ be close enough to the exact solution and that the Jacobian be non-singular and Lipschitz continuous, this iteration will converge to the exact solution at a quadratic rate (Dennis & Schnabel, theorem 5.2.1.). If we make the initial estimate (A 3) and the integration (A 8) acurate enough and stay away from bifurcation points (where the Jacobian is singular), then convergence of this step is practically guaranteed.

We use SPARSPAK to solve each step of (A 9), and a line search algorithm to improve global convergence properties. The structure of the Jacobian in (A 9) is the same as that of $\mathbf{L}$ in (A 8), so the most time-consuming part of the SPARSPAK algorithm – the structure decomposition – needs to be done only once.

A.3. *Numerical errors and convergence*

Two types of numerical errors need to be considered: the discretization error (the difference between the exact analytic solution and the exact solution of the discretized system), and the convergence error (the difference between the numbers actually obtained and the exact solution of the discretized problem). Convergence errors are important in the corrector step only, since those occurring in the predictor steps – initial estimate and integration – are irrelevant when the corrector step converges.

The initial estimate need not be very accurate, as explained above. However, if it is too inaccurate, then the corrector procedure may converge to a different branch or not converge to a solution at all. The initial estimate will be improved as $\epsilon \to 0$ in (A 3), but the integration and corrector steps will lose accuracy as the Jacobian becomes singular near the bifurcation point. We found that with $\epsilon = 0.01$, taking up to 3 terms of the series (A 3) leads to convergence of (A 9) and reasonable accuracy for the subsequent integration.

The convergence errors are determined by the stopping criterion of the corrector step (A 9):

$$\|\mathbf{D}\boldsymbol{\Phi}+\boldsymbol{\Omega}(\boldsymbol{\Phi},\Lambda)\|_2^2 \leqslant \delta^2.$$

The change in $\|\boldsymbol{\Phi}\|$ in the last Newton step is usually considered to be of the same order as the convergence error. For $\delta = 10^{-8}$, the typical value was: $\|\Delta\boldsymbol{\Phi}\| \approx 10^{-5}$. As shown below, this is much smaller than the estimate for the discretization error, and we may therefore treat the computed solutions as 'exact' solutions of the discretized problem.

Equation (A 2) was derived using central differences, and is second-order correct in $\Delta r, \Delta\zeta$. The grid transformations $z \to \zeta$ used have a finite derivative everywhere, and therefore do not affect the order of the truncation error (Kalnay de Rivas 1972); therefore it is considered second order also in Δz. Higher-order accuracy, as well as an estimate for the discretization error, may be obtained by Richardson's extrapolation. Computation was repeated for sample cases with grids having resolutions of (N_r, N_z), where N_r and $N_z \in (10, 20, 40)$: 9 different grids, followed by a two-dimensional extrapolation to $1/N \to 0$. Typical values of the relative difference of the second-order solution from the extrapolated results are presented in figure 18; these differences serve as an estimate for the discretization error.

To further validate the above estimate of the discretization error, we applied the numerical algorithm to a problem having a known solution. The nonlinear function Ω in equation (16) is chosen to be:

$$\Omega(\Phi, r; \Lambda) = \Lambda\Phi + \frac{\Phi^2}{rJ_1(\alpha r)},$$

where J_1 is a Bessel function of order 1 and α is its first zero ($\alpha = 3.8317\ldots$). Equation (16) with this Ω has an analytic solution which is qualitatively similar to the computed (and weakly nonlinear) solitary waves:

$$\Phi(r, z) = \tfrac{3}{2}(\alpha^2 - \Lambda)\, rJ_1(\alpha r)\, \mathrm{sech}^2\,[\tfrac{1}{2}z(\alpha^2 - \Lambda)^{\frac{1}{2}}].$$

This solution bifurcates from the trivial $\Phi = 0$ branch at $\Lambda = \alpha^2$ and increases in magnitude as $\Lambda \to 0$. (This problem does not necessarily correspond to a physical primary flow.) The discretization errors for Φ, μ_{00}, μ_{01} and the first two axial wavenumbers are presented in figure 19.

The error in the perturbation stream function with the 20×20 grid is close to 2% for the test function and less than 1% for the Richardson-extrapolated case. For velocities (computed from the stream function by central differences), the discretization error is larger, but still not exceeding a few percent on a 20×20 grid. The results in figure 18(*b*) are for the axial velocity $w = \partial\psi/r\,\partial r$, which is strongly dependent on r-resolution. The errors in the values of the axial wavenumbers $\beta_n^{\frac{1}{2}}$ and the bifurcation points μ_{nm} are similarly of order 1% for the same level of resolution. The 20×20 grid was therefore the standard in most of our computations.

A.4. *The singularity at* $r = 0$

Equation (16) has a singularity on the axis $r = 0$, and construction of a numerical scheme as well as interpretation of the results should take that singularity into account. The discretization (A 2) makes explicit use of the boundary condition (16*c*) at $r = 0$, and applies (A 1) only to interior grid points; the singularity is thus avoided.

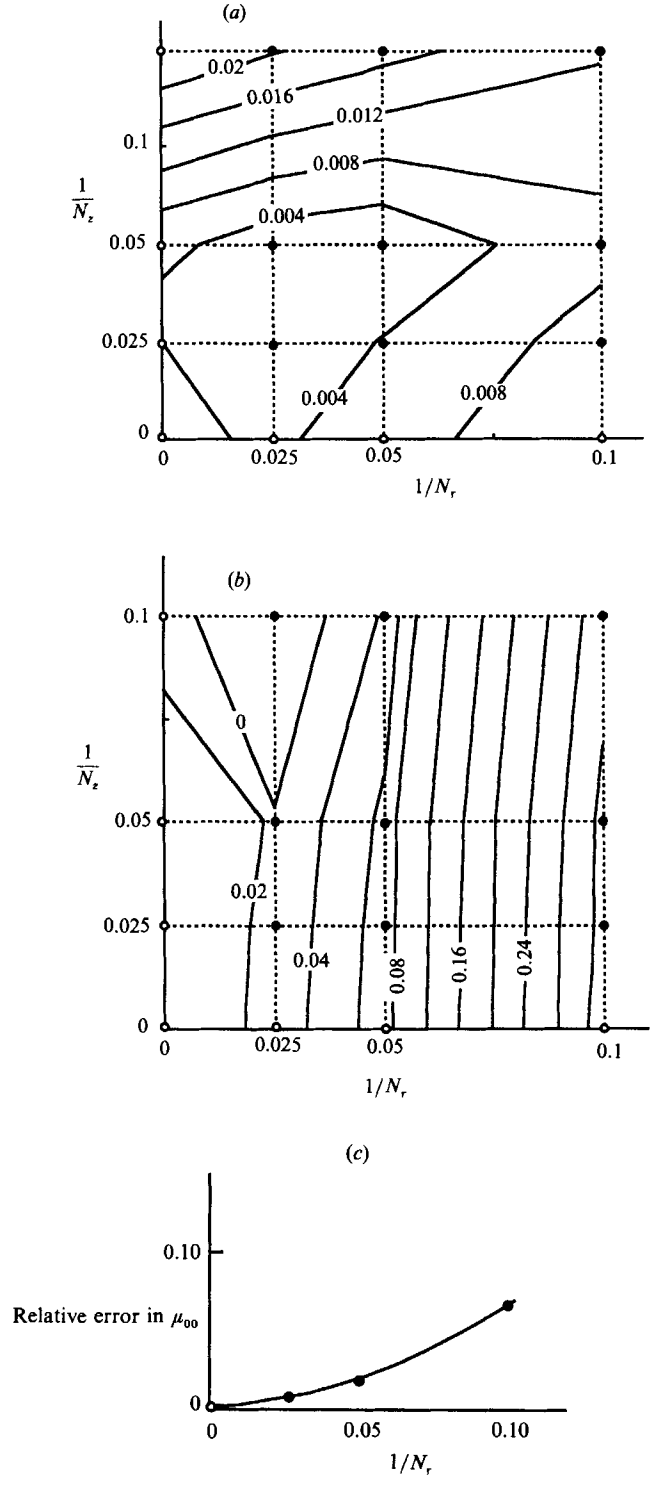

FIGURE 18. Variation with mesh size of errors relative to Richardson-extrapolated values at $A/\mu_{00} = 0.80$: ●, actual computation with this mesh; ○, extrapolated. (*a*) Error in $\Phi(0.3, 0)$, (*b*) error in $w(0, 0)$, (*c*) error in μ_{00}.

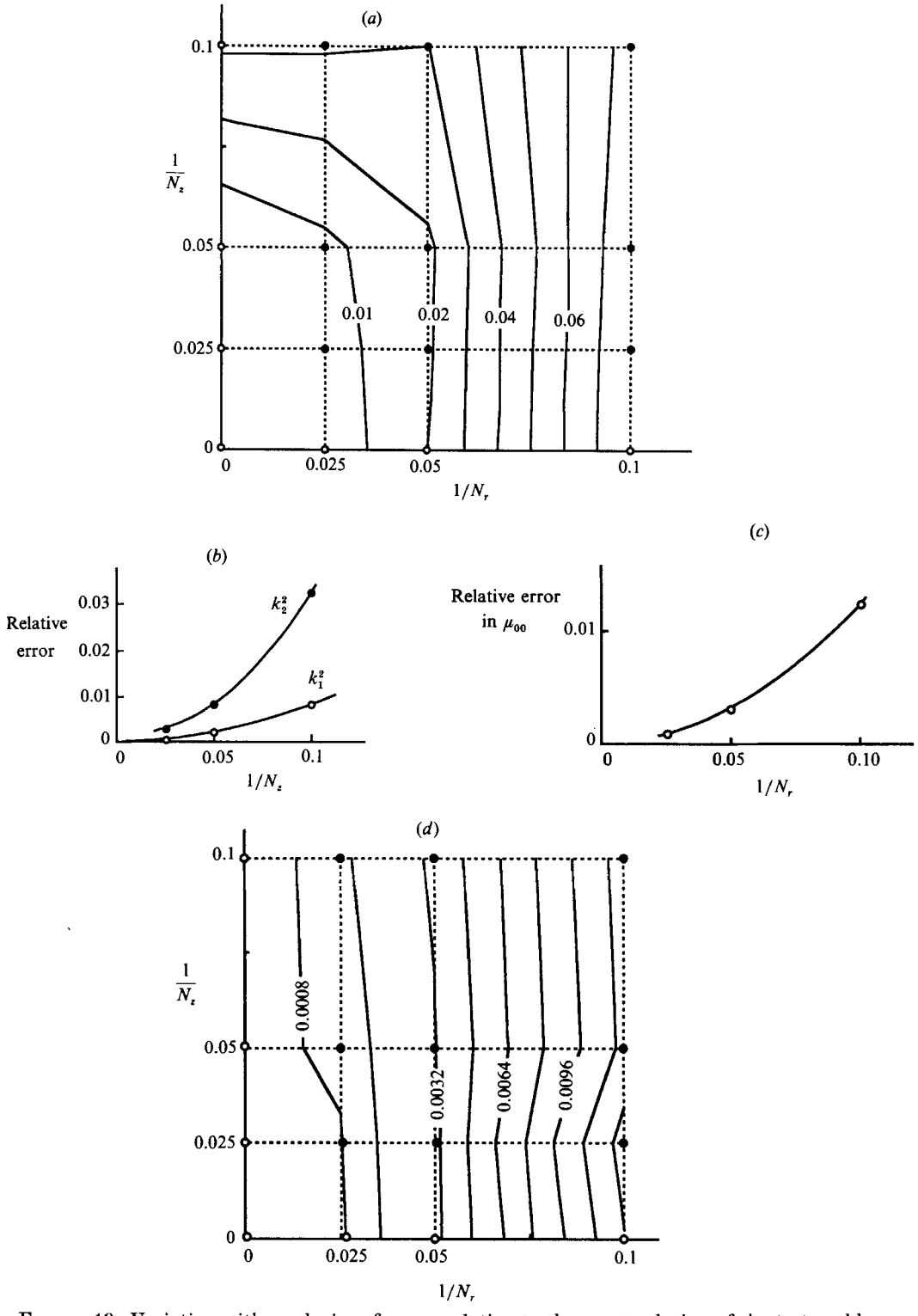

FIGURE 19. Variation with mesh size of errors relative to the exact solution of the test problem: ●, actual computation with this mesh; ○, extrapolated. (*a*) Maximum error in $\Phi(r, z)$ at $\Lambda/\alpha^2 = 0.80$, (*b*) error in axial wavenumbers, (*c*) error in μ_{00}, (*d*) error in μ_{01}.

However, if the grid is refined until $1/r$ becomes very large at the first grid point off the axis, then the matrices involved will become unbalanced and numerical accuracy will deteriorate. In our case such fine grids are not necessary since Richardson's extrapolation seems to show convergence before very large numbers occur.

The singularity is encountered again when we compute the axial velocity at the axis, which is used as a measure of the perturbation size. The definition $w = r^{-1}\partial\psi/\partial r$ cannot be applied directly at $r = 0$; two numerical schemes are used, and the values obtained for $w(0,0)$ agree to within a few percent.

The first method is a quadratic extrapolation of w-values from interior grid points, coupled with the condition $\partial w/\partial r = 0$ at $r = 0$. The quadratic function satisfying this condition and passing through the first two interior grid points is

$$\tilde{w}(r) = \tfrac{1}{3}w(\Delta r)\left[4-\left(\frac{r}{\Delta r}\right)^2\right]+\tfrac{1}{3}w(2\Delta r)\left[\left(\frac{r}{\Delta r}\right)^2-1\right],$$

leading to

$$\tilde{w}(0) = \frac{4w(\Delta r)-w(2\Delta r)}{3}.$$

The second method applied Stokes' theorem to a rectangular loop of dimensions $(\delta r, \delta z)$ touching the axis $r = 0$ and centred about the line of symmetry $z = 0$. To reduce the error associated with numerical integration over a finite rectangle, we let $\delta z \to 0$ and obtain a balance involving r-integration only. The vorticity integral can be expanded in powers of δz, η being the azimuthal component of the vorticity:

$$\int_s \boldsymbol{\omega}\cdot\mathrm{d}\boldsymbol{s} = \int_0^{\delta r}\int_{-\delta z/2}^{\delta z/2}\left[\eta(r,0)+z\frac{\partial\eta}{\partial z}(r,0)+\ldots\right]\mathrm{d}z\,\mathrm{d}r = \delta z\int_0^{\delta r}\eta(r,0)\,\mathrm{d}r+O(\delta z^2).$$

A similar expansion is done for the recirculation integrals:

$$\oint \boldsymbol{u}\cdot\mathrm{d}\boldsymbol{l} = \int_{-\delta z/2}^{\delta z/2}[w(0,z)-w(\delta r,z)]\,\mathrm{d}z+\int_0^{\delta r}[u(r,\tfrac{1}{2}\delta z)-u(r,-\tfrac{1}{2}\delta z)]\,\mathrm{d}r$$

$$= \delta z\left[w(0,0)-w(\delta r,0)-\int_0^{\delta r}\frac{1}{r}\frac{\partial^2\psi}{\partial z^2}(r,0)\,\mathrm{d}r\right]+O(\delta z^2).$$

Comparing the leading terms in δz, we obtain

$$w(0,0) = w(\delta r,0)+\int_0^{\delta r}\left[\eta(r,0)+\frac{1}{r}\frac{\partial^2\psi}{\partial z^2}(r,0)\right]\mathrm{d}r.$$

The integral was computed using the Simpson $\frac{1}{3}$-rule, and the two expressions for $w(0,0)$ were compared for $\delta r = \Delta r$ and $2\Delta r$. The differences were of order 1% in most cases, and increased up to 5% only as $\Lambda \to \mu$ (where the perturbation is small and roundoff error becomes significant) and as $\Lambda \to 0$ (where large radial gradients require increased resolution). We therefore used the simpler quadratic extrapolation form throughout. This comparison also serves as an additional check on the convergence of the numerical results near the singular line $r = 0$.

Appendix B. Singular limit of zero swirl

For the specifying flow (34) that we have been using as example, the zero-swirl limit $\Lambda = 0$ is irrotational, and the constant-speed flow $\psi = \frac{1}{2}r^2$ is unique. Therefore no differentiable solutions exist except for the specifying flow. On the other hand, our

numerical results suggest that the limit $\Lambda \to 0+$ along the principal columnar branch develops a strong shear layer tending in the limit to a vortex sheet separating two piecewise irrotational limiting flows, in each section of which the flow is oppositely directed and of uniform infinite speed! We explore this bizarre situation by an asymptotic development that seems to fit with the numerical findings, and which gives the asymptotic dependence of the velocity levels, and of the shear layer location and thickness on Λ.

It is convenient here to work with the total stream function ψ, governed by (11), rather than the perturbation from the specifying flow. For the specifying flow (34), the limit of equation (11) when $\Lambda = 0$ is $\mathrm{D}^2\psi = 0$, with a solution that is linear in r^2. We assume the existence of a discontinuity in this limit, located at $r = r_*$, at which the stream function reaches its minimum value, $\psi(r_*) \equiv -\psi_*(\Lambda)$. The analysis of this section is simplified by the change of variable

$$\eta = \tfrac{1}{2}r^2.$$

Then we may write (using the condition that $\psi = 0$ at $\eta = 0$ and $\psi = \frac{1}{2}$ at $\eta = \frac{1}{2}$, and defining $\eta_* = \frac{1}{2}r_*^2$)

$$\left.\begin{aligned} \psi &= C\eta \quad \text{for} \quad \eta - \eta_* < 0, \\ \psi &= D(\eta - \tfrac{1}{2}) + \tfrac{1}{2} \quad \text{for} \quad \eta - \eta_* > 0. \end{aligned}\right\} \tag{B 1}$$

For Λ very small but not zero, we assume the existence of a single internal layer, centred on η_* and with a thickness $\delta(\Lambda)$ that tends to zero as $\Lambda \to 0+$, that joins these two constant-speed solutions. Furthermore, the numerical results suggest that $\psi_*(\Lambda) \to \infty$ as $\Lambda \to 0$, and we also assume this.

The solution to the outer problem has been described above, and now we seek a structure to the internal boundary layer separating the two irrotational regions. It is important (and easy to show) that $\mathrm{D}^2\psi = 0$ to *all* algebraic orders in the small parameter in the outer regions, so that the full outer expansions retain the form (B 1), with the coefficients of η being functions of Λ. The point η_* and the constants C and D occurring in the outer problem are not yet known and must be determined by matching with this internal boundary layer. The argument is reminiscent of activation energy asymptotics (see Buckmaster & Ludford 1982). Stretch the radial scale near $\eta = \eta_*$, by taking

$$\eta \equiv \eta_* + \delta X = \eta_*(1 + \mu X), \quad \mu \equiv \delta/\eta_*, \tag{B 2}$$

where δ is the lengthscale appropriate in the layer and it is assumed that $\delta(\Lambda) \to 0$ as $\Lambda \to 0$. Near η_* the stream function is continuous and the appropriate scale for it is $-\psi_*(\Lambda)$, so we write

$$\psi(\eta_* + \delta X) = -\psi_*(\Lambda)\,[1 + \epsilon(\Lambda)\, y(X;\Lambda)] \tag{B 3}$$

in the layer, where the asymptotically small parameter $\epsilon(\Lambda)$, like the parameters $\delta(\Lambda)$ and $\psi_*(\Lambda)$, remain to be identified. From the definition of $-\psi_*(\Lambda)$ as the extreme value of ψ, we must have

$$y(0;\Lambda) = y'(0;\Lambda) = 0, \tag{B 4}$$

where $(\,)' \equiv \mathrm{d}y/\mathrm{d}X$, and we also have $y \leqslant 0$ for all X. We substitute the ansatz (B 1)–(B 3) into (11) and invoke (34). This yields

$$y'' + \frac{2\alpha\Lambda\delta^2}{\epsilon\psi_*}\mathscr{G}(y) = 0,$$

where

$$\mathscr{G}(y) \equiv \left(\frac{1}{2\eta}+\frac{1}{2\psi_*(1+\epsilon y)}\right)\mathrm{e}^{4\alpha\psi_*(1+\epsilon y)}(1-\mathrm{e}^{-2\alpha\psi_*(1+\epsilon y)}).$$

The distinguished limit arises for $2\alpha\psi_*\epsilon$ and $2\alpha\Lambda\delta^2\mathrm{e}^{4\alpha\psi_*}/2\eta_*$ both $O(1)$, and we therefore set

$$2\alpha\psi_*\epsilon = 4\alpha^2\Lambda\delta^2\mathrm{e}^{4\alpha\psi_*}/2\eta_* = 1, \tag{B 5}$$

which leads to the equation

$$y''+\left[\frac{1}{1+\mu X}+\frac{2\eta_*\alpha\epsilon}{1+\epsilon y}\right]\mathrm{e}^{2y} = 0, \tag{B 6}$$

with exponentially small error. We may now look for a solution to this inner problem in the form of power series in the small parameter. It is more convenient in the analysis to regard ϵ as the controlling small parameter rather than Λ, and so we take

$$y = y_0+\epsilon y_1+\ldots, \tag{B 7}$$

$$\mu = \mu_1\epsilon+\mu_2\epsilon^2+\ldots, \tag{B 8}$$

$$1/2\eta_* = \gamma_0+\gamma_1\epsilon+\ldots, \tag{B 9}$$

and the slightly unconventional form of the last expansion makes the matching with the outer solution simpler.

The equations for first two coefficients, y_0 and y_1, of (B 7) are

$$y_0''+\mathrm{e}^{2y_0} = 0, \tag{B 10}$$

$$y_1''+2\,\mathrm{e}^{2y_0}y_1 = \left[\mu_1 X-\frac{\alpha}{\gamma_0}\right]\mathrm{e}^{2y_0}. \tag{B11}$$

The solution to (B 10) satisfying (B 4) is

$$y_0(X) = \ln\operatorname{sech}(X), \tag{B 12a}$$

and the solution to (B 11) is

$$y_1(X) = \frac{1}{2}\left[\mu_1(X-\tanh X)-\frac{\alpha}{\gamma_0}X\tanh X\right] \tag{B 12b}$$

We now match the stream function in the inner region with the two outer regions. Matching to second order in ϵ yields

$$\frac{1}{2\eta_*} = (2+\epsilon(1+\alpha))+\gamma_2\epsilon^2; \tag{B 13a}$$

$$C = -\frac{1}{2\alpha\epsilon\eta_*}(1+\epsilon\ln 2+\tfrac{1}{2}\epsilon^2), \quad D = -\frac{1}{2\alpha\epsilon\eta_*}(-1+\epsilon(1-\ln 2)+\epsilon^2 b_2) \tag{B 13b, c}$$

$$\mu = \epsilon+\epsilon^2(\tfrac{1}{2}+\tfrac{1}{4}\alpha-\ln 2), \quad \delta = \eta_*\mu, \tag{B 13d, e}$$

and from these we can find

$$\Lambda = 2\eta_*(2\alpha\delta\,\mathrm{e}^{2\alpha/\epsilon})^{-2}. \tag{B 13f}$$

The numbers γ_2 in (B 13a) and b_2 in (B 13c) are undetermined at this order, and therefore our solution is completely determined only to one order less than we have

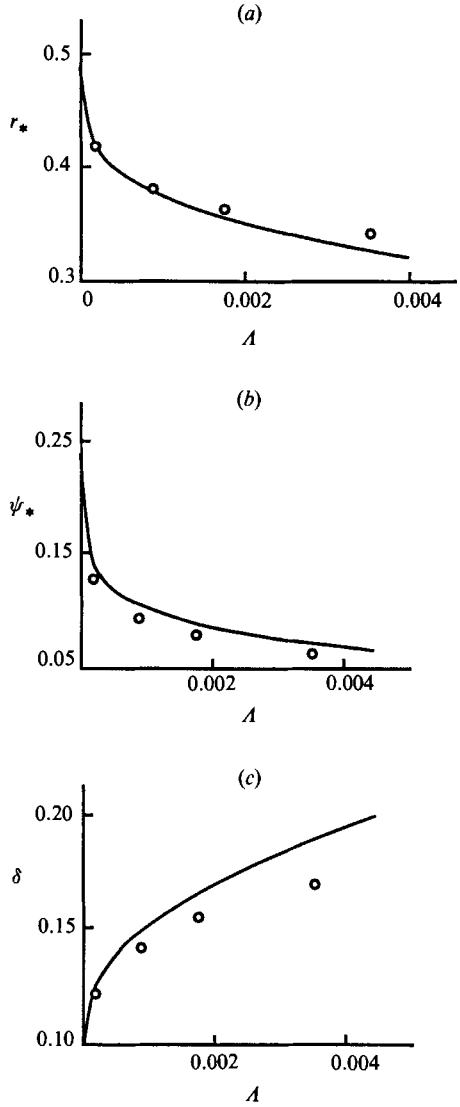

FIGURE 20. Comparison of computed (○) and asymptotic (——) solutions in the limit $A \to 0$ on the principal branch. (*a*) Location of the boundary layer, (*b*) maximum of the stream function ψ_*, (*c*) layer thickness δ.

shown – on the other hand, it is necessary to match at the level shown to accurately determine the solution to that order (i.e. to within an error of $O(\epsilon)$).

The composite expansion for ψ constructed from (B 1)–(B 3), (B 12), (B 13) is

$$\psi = -\frac{1}{2\alpha\epsilon}\left\{(1+\epsilon\ln 2)\frac{\eta}{\eta_*}H(\eta_*-\eta)+(-1+\epsilon(1-\ln 2)\frac{\eta-\frac{1}{2}}{\eta_*}H(\eta-\eta_*)\right.$$
$$\left.+\epsilon\left[\ln\tfrac{1}{2}\operatorname{sech}\left(\frac{\eta-\eta_*}{\delta}\right)\right]+\left|\frac{\eta-\eta_*}{\delta}\right|\right\}+\tfrac{1}{2}H(\eta-\eta_*); \quad \psi(r_*) = -\frac{1}{2\alpha\epsilon}, \quad \text{(B 14)}$$

where $H(t)$ is the unit function, $H(t) = 1$ for $t > 0$, $H(0) = \frac{1}{2}$, and $H(t) = 0$ for $t < 0$.

Equations (B 13) give δ, r_*, and A as a function of the parameter ϵ, and from them

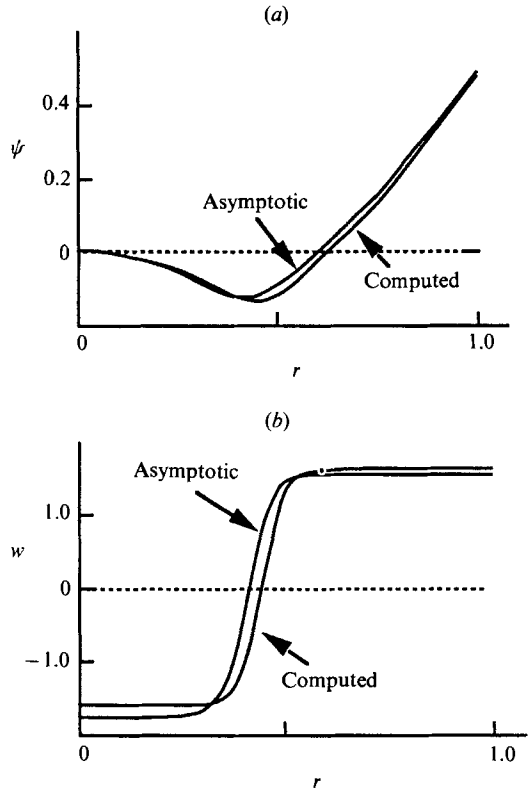

FIGURE 21. Comparison of computed and asymptotic velocity profiles for the principal branch, at $\Lambda = 0.001\mu_{00}$.

the dependence of δ and r_* on Λ can be evaluated to yield the desired asymptotic relationship between these parameters as $\Lambda \to 0$. As seen in figure 20, the differences between the computed and the asymptotic values are only a few percent for $\Lambda = 0.01$. The asymptotic solution (B 14) is compared in figure 21 to the computed stream function and axial velocity for $\Lambda = 1.769 \times 10^{-4}$. The agreement is quite good, considering the fact that $\psi_* = 0.13$, not yet large as the analysis assumes, meaning that the asymptotic relation is good far beyond its expected region of $|\psi_*| \gg 1$.

The azimuthal velocity component, v, is exponentially small except in the shear layer. The shear layer is a concentrated region of vorticity, with both axial vorticity arising from the swirl as well as azimuthal vorticity arising from the variation in axial velocity across the layer present. As $\Lambda \to 0$, the swirl component $v \to 0$ in the layer as $\Lambda^{\frac{1}{2}}/|\ln \Lambda|$, which is very much slower than Λ.

REFERENCES

BATCHELOR, G. K. 1956 On steady laminar flow with closed streamlines at large Reynolds number. *J. Fluid Mech.* **1**, 177–190.

BATCHELOR, G. K. 1967 *Introduction to Fluid Dynamics.* Cambridge University Press.

BENJAMIN, T. B. 1962 Theory of the vortex breakdown phenomenon. *J. Fluid Mech.* **14**, 593–629.

BENJAMIN, T. B. 1967 Some developments in the theory of vortex breakdown. *J. Fluid Mech.* **28**, 65–84.

BRAGG, S. L. & HAWTHORNE, W. R. 1950 Some exact solutions of the flow through annular cascade actuator discs. *J. Aero. Sci.* **17**, 243–249.

BUCKMASTER, J. S. & LUDFORD, G. S. S. 1982 *Theory of Laminar Flames.* Cambridge University Press.

COURANT, R. & HILBERT, D. 1953 *Methods of Mathematical Physics*, Vol. 1. Interscience.

DENNIS, J. E. & SCHNABEL, R. B. 1983 *Numerical Methods for Unconstrained Optimization and Nonlinear Equations.* Prentice-Hall.

DONGARRA, J. J. 1979 *Linpack User's Guide.* Society for Industrial and Applied Mathematics.

ESCUDIER, M. P. 1984 Observations of the flow produced in a cylindrical container by a rotating endwall. *Exps Fluids* **2**, 189–196.

FALER, J. H. & LEIBOVICH, S. 1977 Disrupted states of vortex flow and vortex breakdown. *Phys. Fluids* **20**, 1385–1400.

FALER, J. H. & LEIBOVICH, S. 1978 An experimental map of the internal structure of a vortex breakdown. *J. Fluid Mech.* **86**, 313–335.

FIEDLER, B. B. & ROTUNNO, R. 1986 A theory for the maximum windspeeds in tornado-like vortices. *J. Atmos. Sci.* **43**, 2328–2340.

FRAENKEL, L. E. 1956 On the flow of rotating fluid past bodies in a pipe. *Proc. R. Soc. Lond.* A **233**, 506–526.

FRAENKEL, L. E. 1967 On Benjamin's theory of conjugate vortex flows. *J. Fluid Mech.* **28**, 85–96.

GARG, A. K. & LEIBOVICH, S. 1979 Spectral characteristics of vortex breakdown flowfields. *Phys. Fluids* **22**, 2053–2064.

GEORGE, A., LIU, J. & NG, E. 1980 *User Guide for SPARSPAK.* University of Waterloo.

HAFEZ, M., AHMAD, J., KURUVILA, G. & SALAS, M. D. 1987 *Vortex breakdown simulation. AIAA* 87-1343, Honolulu, Hawaii.

HAFEZ, M. & SALAS, M. 1985 Vortex breakdown simulation based on a nonlinear inviscid model. In *Studies of Vortex Dominated Flows* (ed. M. Y. Hussaini & M. D. Salas), pp. 76–82.

HARVEY, J. K. 1962 Some observations of the vortex breakdown phenomenon. *J. Fluid Mech.* **14**, 585–592.

HOWARD, L. & GUPTA, A. S. 1962 On the hydrodynamic and hydromagnetic stability of swirling flows. *J. Fluid Mech.* **14**, 463–476.

KALNAY DE RIVAS, E. 1972 On the use of nonuniform grids in finite-difference equations. *J. Comput. Phys.* **10**, 202–210.

KELLER, H. B. 1977 Numerical solution of bifurcation and nonlinear eigenvalue problems. In *Applications of Bifurcation Theory* (ed. P. H. Rabinowitz), pp. 359–384. Academic.

KELLER, J. J., EGLI, W. & EXLEY, J. 1985 Force- and loss-free transitions between flow states. *Z. Agnew. Math. Phys.* **36**, 854–889.

KUBICEK, M. & MAREK, M. 1983 *Computational Methods in Bifurcation Theory and Dissipative Structures.* Springer.

LEIBOVICH, S. 1968 Axially-symmetric eddies embedded in a rotational stream. *J. Fluid Mech.* **32**, 529–548.

LEIBOVICH, S. 1970 Weakly nonlinear waves in rotating fluids. *J. Fluid Mech.* **42**, 803–822.

LEIBOVICH, S. 1978 The structure of vortex breakdown. *Ann. Rev. Fluid Mech.* **10**, 221–246.

LEIBOVICH, S. 1979 Waves in parallel or swirling stratified shear flows. *J. Fluid Mech.* **93**, 401–412.

LEIBOVICH, S. 1983 Vortex stability and breakdown. In *Aerodynamics of Vortical Type Flows in Three Dimensions* (ed. A. D. Young). *AGARD Conf. Proc.* 342 (NATO), *Paper* 23 (herein referred to as L).

LEIBOVICH, S. 1984 Vortex stability and breakdown: Survey and extension. *AIAA J.* **22**, 1192–1206 (herein referrred to as L).

LEIBOVICH, S. 1985 Waves and bifurcations in vortex filaments. In *Studies of Vortex Dominated Flows* (ed. M. Y. Hussaini & M. D. Salas), pp. 3–15. Springer.

LEIBOVICH, S. 1987 Fully nonlinear structures, wavetrains, and solitary waves in vortex filaments. In *Nonlinear Wave Interactions in Fluids* (ed. R. W. Miksad, T. R. Akylas & T. Herbert), pp. 67–70. ASME.

LEIBOVICH, S., BROWN, S. N. & PATEL, Y. 1986 Bending waves on inviscid columnar vortices. *J. Fluid Mech.* **173**, 596–624.

LEIBOVICH, S. & STEWARTSON, K. 1983 A sufficient condition for the instability of columnar vortices. *J. Fluid Mech.* **126**, 335–356.

LONG, R. R. 1953 Steady motion around axisymmetric obstacle moving along the axis of a rotating liquid. *J. Met.* **10**, 197–203.

LUGT, H. J. & ABBOUD, M. 1987 Axisymmetric vortex breakdown in rotating fluid within a container. *J. Fluid Mech.* **179**, 179–200.

MAXWORTHY, T., MORY, M. & HOPFINGER, E. 1983 Waves on vortex cores and their relation to vortex breakdown. In *Aerodynamics of Vortical Type Flows in Three Dimensions* (ed. A. D. Young). *AGARD Conf. Proc.* 342 (NATO), *Paper* 29.

PRANDTL, L. 1904 Über Flüssigkeitsbewegung bei sehr kleiner Reibung, *3rd Intl Congr. Mathematicians (Heidelberg)*, pp. 484–491. Leipzig: B. G. Teubner.

PRESS, W. H., FLANNERY, B. P., TEUKOLSKY, S. A. & VETTERLING, W. T. 1986 *Numerical Recipes.* Cambridge University Press.

RANDALL, J. D. & LEIBOVICH, S. 1973 The critical state: a trapped wave model of vortex breakdown. *J. Fluid Mech.* **53**, 481–493 (herein referred to as RL).

RAYLEIGH, LORD 1916 On the dynamics of revolving fluids. *Proc. R. Soc. Lond.* A **93**, 148–154.

RONNENBERG, B. 1977 Ein selbstjustierendes 3-Komponenten-Laserdoppleranemometer nach dem Vergleichsstrahlverfahren, angewandt für Untersuchungen in einer stationären zylindersymmetrischen Drehströmung mit einem Rüchstromgebiet. *Max-Planck Inst. für Strömungsforschung, Göttingen, Bericht* 20.

SARPKAYA, T. 1971 On stationary and travelling vortex breakdowns. *J. Fluid Mech.* **45**, 545–559.

SMITH, B. T., BOYLE, J. M., DONGARRA, J., GARBOW, B., IKEBE, I., KLEMA, V. C. & MOLER, C. B. 1976 *Matrix Eigensystem Routines – EISPACK Guide*, 2nd edn, Lectures Notes in Computer Science, vol. 6. Springer.

SQUIRE, H. B. 1956 Rotating fluids. *Surveys in Mechanics* (ed. G. K. Batchelor & R. M. Davies), pp. 139–161. Cambridge University Press.

SYNGE, J. L. 1933 The stability of heterogeneous liquids. *Trans. R. Soc. Can.* **27**, 1–18.

SZERI, A. J. 1988 Nonlinear stability of axisymmetric swirling flow. Ph.D. dissertation, Cornell University, Ithaca, NY.

SZERI, A. J. & HOLMES, P. 1988 Nonlinear stability of axisymmetric swirling flows. *Phil. Trans. R. Soc. Lond.* A **326**, 327–354.

VOGEL, H. U. 1968 Experimentelle Ergebnisse über die laminare Strömung in einem zylindrischen Gehäuse mit darin rotierender Scheibe. *Max-Planck Inst. für Strömungsforschung, Göttingen, Bericht* 6.

YIH, C. S. 1965 *Dynamics of Nonhomogeneous Fluids.* Academic.